Lappeenranta University of Technology

LUT School of Energy Systems

Energy Technology

Ville Ottelin

Modelling of a board machine’s heat recovery system

Master’s Thesis

Examiners: Professor, D.Sc. (Tech.) Esa Vakkilainen

D.Sc. (Tech.) Jussi Saari

Supervisors: Lic.Sc. (Tech.) Jari Kääriäinen

M.Sc. (Tech.) Petri Norri

ABSTRACT

Lappeenranta University of Technology

LUT School of Energy Systems

Energy Technology

Ville Ottelin

Modelling of a board machine's heat recovery system

Master's Thesis

2019

75 pages, 11 figures, 12 tables and 3 appendices

Examiners: Esa Vakkilainen

Jussi Saari

Keywords: board machine, heat recovery, modelling, MATLAB, Simulink

Valmet is creating a digital twin for a board machine and its heat recovery system is modelled in this master's thesis. The objective of the thesis is to create a model for the heat recovery system that can be utilized in customer application and in process designing. In addition, a preliminary design for the customer application is created.

The boardmaking process, hood operation and board machine's heat recovery system are presented based on the literature and web sources. Essential equations for heat recovery modelling are presented before explaining the structure of the created MATLAB models. The model's accuracy is validated by comparing simulation results with previous models. As a result, the air-to-air unit model has more uncertainty than the air-to-water unit. Input parameters' influence is researched, showing that the exhaust air humidity and the absorbing flow temperature are the most influential parameters on the recovered energy.

Model accuracy is sufficient for condition monitoring and trouble-shooting, but more verification is needed for design utilization. Additional measurements must be added to the current board machines to enable the model's validation.

TIIVISTELMÄ

Lappeenrannan teknillinen yliopisto

LUT Energiajärjestelmät

Energiatekniikan koulutusohjelma

Ville Ottelin

Kartonkikoneen lämmöntalteenottojärjestelmän mallintaminen

Diplomityö

2019

75 sivua, 11 kuvaa, 12 taulukkoa and 3 liitettä

Tarkastajat: Esa Vakkilainen

Jussi Saari

Hakusanat: kartonkikone, lämmöntalteenotto, mallintaminen, MATLAB, Simulink

Valmet on tekemässä digitaalista kaksosta koko kartonkikoneelle, ja tämän vuoksi tässä diplomityössä tehtiin malli lämmöntalteenottojärjestelmälle. Työn tavoitteena oli luoda malli, jota voidaan hyödyntää asiakassovelluksessa sekä prosessisuunnitellussa. Lisäksi työhön kuului asiakassovelluksen alustava suunnittelu.

Työn kirjallisuusosassa esiteltiin kartongin valmistuksen eri vaiheet sekä huuvan ja lämmöntalteenoton toiminta. Lähteinä käytettiin alan kirjallisuutta ja internetaineistoja. Lämmöntalteenoton keskeisimmät kaavat esitettiin ennen luodun MATLAB mallin toiminnan esittelyä. Mallin tarkkuutta selvitettiin vertaamalla mallin tuloksia aiempiin malleihin. Ilma-ilmakennon mallinnus todetaan epävarmemmaksi kuin ilma-vesikennon. Parametrien vaikutusta tutkittiin, ja poistoilman kosteuden ja lämpöä vastaanottavan virran lämpötilan huomataan vaikuttavan eniten talteenotettuun energiaan.

Rakennetun mallin tarkkuus on riittävä, jotta sitä voidaan hyödyntää kunnon valvonnassa ja ongelmanratkaisussa, mutta lisätutkimusta tarvitaan ennen mitoituskäyttöä. Lisää mittauksia tarvitaan mallin validointia varten.

ACKNOWLEDGEMENTS

I would like to thank Valmet for this opportunity to do this master's thesis and learn more about heat transfer modelling. It was interesting to study more about board machine's air systems and increase my knowledge on boardmaking process. I am grateful for the support from Valmet. Special thanks to Jari Kääriäinen, Petri Norri, Hans Sundqvist and everybody else who has been involved in this project.

I would also like to thank Professor Esa Vakkilainen for instructions and guidance during the work and whole Lappeenranta University of Technology for the past five years.

Jyväskylä 4.8.2019

Ville Ottelin

TABLE OF CONTENTS

NOMENCLATURE

Roman Letters

A	area	m^2
C	coefficient	-
c_p	specific heat capacity	J/kg K
D	diameter, mass diffusion coefficient	m, cm^2/s
h	convection coefficient	W/m^2 K
k	mass transfer coefficient	m/s
L	characteristic length	m
l	latent heat	J/kg
M	molecular weight	g/mol
m	coefficient	-
$\dot{m}$	flow rate	kg/s
n	coefficient	-
P	perimeter	m
p	pressure	bar, Pa
Q	heat transfer rate	W
q	convective heat flux	W/m^2

R	universal gas constant	J/mol K
s	surface thickness	mm
T	temperature	K, °C
U	overall heat transfer coefficient	W/m^2 K
v	velocity	m/s
x	absolute humidity	g H_2O/kg d.a.

Greek Letters

γ	mole fraction	-
λ	thermal conductivity	W/m K
μ	viscosity	kg/s m
ρ	density	kg/m^3

Dimensionless Numbers

EFF	efficiency coefficient
Le	Lewis number
Nu	Nusselt number
Pr	Prandtl number
Re	Reynolds number

Subscripts

0	theoretical
1	component
12	from component 1 to component 2
2	component
21	from component 2 to component 1
3	component
4	component
A	component
B	component
c	cross-sectional
D	diameter
d.a.	dry air
dim	dimensioned
ev	evaporated
h	hydraulic
i	component
j	component

mh	machine hall
pw	process water
rec	recovered
s	surface
sat	saturated
sup	supply
vap	vapor
∞	surrounding

Abbreviations

AHR	aqua heat recovery unit
AWS	Amazon Web Services
CHR	conventional heat recovery unit
KPI	key performance indicator
MVP	minimum viable product
OCC	old corrugated containers

1 INTRODUCTION

1.1 Background

Sustainability is an important factor in today's industry. One of the biggest aspects in sustainability is energy efficiency. Energy usage is usually a significant cost, which also causes greenhouse gases, making the optimization of energy consumption a key parameter in the economic and environmental strategy of businesses. (Portney 2015, 37)

The heat recovery system is a critical part of the board machine's overall energy efficiency. Heat recovery systems' heat exchangers transfer thermal power from exhaust air to supply air and water flows. A heat recovery system can generate up to 50 % of the paper machines' primary energy and energy constitutes in average of 16 % of operational costs in boardmaking. (Sivill et al., 2005) In other words, minor enhancements in heat recovery could bring big savings in energy costs.

Digitalization is transforming how companies must operate. The accessibility of data is improved as the measuring equipment is gotten cheaper and the processing power of computers has increased. Companies' challenge is how to utilize data for customer applications. A solution to this problem is a digital twin, which is a concept where a real time digital replica is made from a physical component, product or process. A digital twin comprises all the variables in the life-cycle of the subject. One of its uses is to model real processes for finding optimum working conditions. (Standish, 2018)

1.2 Objectives of thesis

Valmet is creating a digital twin for the board machine. The objective of this thesis is to create a model for the board machine's heat recovery system that will serve as a core for the digital twin. The digital twin will then be used in a Minimum Viable Product (MVP) customer application for heat recovery. The application will be used internally as a simulator and support tool for trouble-shooting and externally as an on-line customer application, which indicates the condition of the heat recovery system and guides the operator in running the system properly. This enables intelligent controlling options, which help customers to optimize their energy usage and save money. One of the

requirements for the model is to have a short computational time, which is necessary for an on-line application. The model will also be used as a dimensioning tool for system designing if the model accuracy is sufficient.

This thesis has three objectives:

1. To create a model for a heat recovery system that indicates system's condition and one that can be converted for an on-line customer application;
2. To create a preliminary design for a customer application;
3. To create a model that can be utilized in heat recovery system designing.

1.3 Structure of thesis

This thesis presents a typical board machine in the chapter 2 by explaining the functioning of different machine sections. Chapter 3 consists of a description of the drying section's ventilation system and explaining the operation of the hood, which covers the drying section. Chapter 4 introduces theory of heat recovery in board machine, as well as typical heat exchanger units used in board machines. Concept of a digital twin, heat transfer equations and heat recovery system modelling in the Simulink environment are presented in chapter 5. Chapter 6 presents the results of the simulations. The created model is compared with another model and simulation tool and the influence of certain parameters is researched. Results are presented mainly in tables. Chapter 7 describes the designed structure of the customer application. The conclusions and findings of this thesis are in the chapter 8, which describes possibilities for utilization. In addition, challenges and future discussion topics are discussed in section 8.3. Thesis is summarized in chapter 9.

1.4 Methods of thesis

The references used in the theory part of this thesis are literature about industry, previous studies and internet sources. In addition to other references, Valmet's internal resources are utilized for the modelling part, and previously developed models are used for providing reference data for validation. A model for heat recovery is created with MATLAB and codes are incorporated to Simulink blocks.

2 BOARDMAKING

This chapter introduces the operation of the board machine. The machine is typically divided into different sections based on their operation principles and purposes. The basic functioning of these sections is explained. This chapter's goal is to explain how board machines operate. The layout of a typical board machine is presented in figure 2.1 where the pulp is fed into the first machine section through the headbox in the top left-hand corner of the figure and the finished paperboard is wound on the reel in the bottom center of the figure. The winder is presented in the bottom right-hand corner of the figure.

Boardmaking consists of two main stages: preparing sufficient pulp, and drying and processing this pulp to create a finished cardboard. This thesis focuses on the machine section, but the basic principles of pulping and stock preparation are also explained. The machine is typically divided into dry and wet ends. The wet end consists of the headbox, wire and press sections. It is where the sheet is formed from the stock and most of the water is removed. The dry end is the second part of the machine, which consists of the rest of the machine from the drying section to the reeling. At the dry end, the sheet's removable moisture is removed by evaporation. (Glossary of Papermaking Terms, 2016)

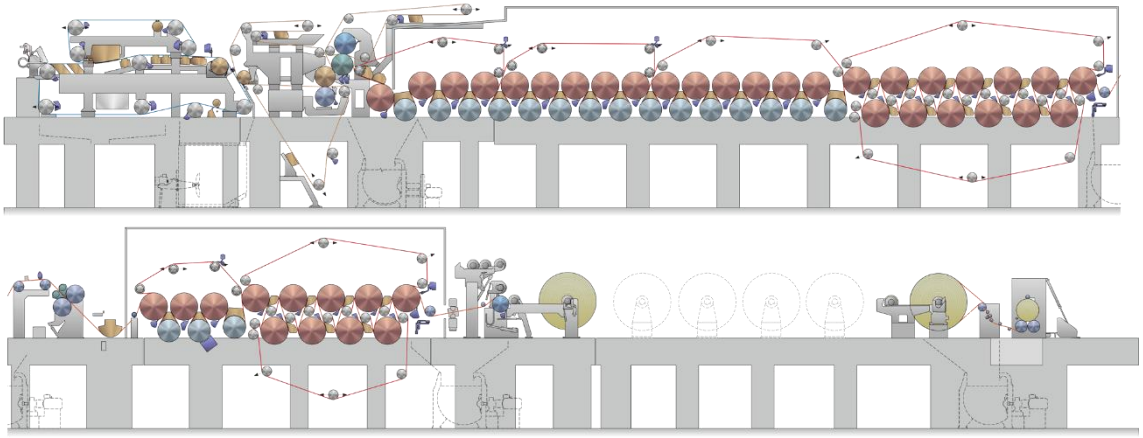

Figure 2.1. Typical layout of a board machine (Valmet Internal).

2.1 Pulping and stock preparation

Boardmaking starts with the production of pulp in a pulp mill. In pulping, fibers are separated from the raw materials creating a pulp. There are many different pulping methods, and the most suitable is selected based on the produced paper or board grades.

Chemical pulping and thermomechanical pulping (TMP) are the two most used methods in boardmaking. (The Pulp and Paper Making Processes, 1996)

Chemical pulping dissolves lignin from the middle lamella through chemical reactions, which free fibers from the wood. More than 60 % of wood can be converted to pulp, which has 10 % lignin content. In the pulping process, the wood is submerged in the cooking liquid, where chemical reactions on the wood surfaces liberates the fibers by removing the lignin. In chemical pulping, mechanical work is either unnecessary, or only slightly necessary. The most utilized chemical pulping method is the kraft method. Its benefits are high energy efficiency and wide-ranging applications. (Fardim 2011, 195) In the kraft method, deaerated wood chips are placed in a digester where cooking liquid is poured onto them to submerge. The liquid consists of white and black liquors. Thus, the active components are OH- and HS- ions. The cooking liquid temperature is 80-100 ℃ at the start, and it is heated to 150-170 ℃. The cooking continues until enough lignin is dissolved from the chips. (Fardim 2011, 203)

Thermomechanical pulping removes fibers from the wood by a combination of heating and mechanical work. The chips are heated with steam and then washed with hot circulation water before they are refined in refiners. In TMP, chips are processed typically in two high pressure, high temperature refiners. The over pressure is 300-500 kPa and the temperature is 143-158 ℃. The refined chips are screened before the accept is dewatered to complete a pulp. (Lönnberg 2009, 177-178)

In modern boardmaking, not all the fibers are separated from the wood by the typical pulping process. Some of the fibers are obtained from recycling. The old corrugated containers (OCC) are recycled and recovered fibers replace virgin fiber. More than 50 % of the fibers in produced cardboard are recycled. The benefits of using the recycled fibers are a lower production cost and lower water consumption compared to virgin fibers, but the strength properties of the fiber are deteriorating with recycling. (Gulsoy et al., 2013)

Produced pulp contains water, fibers and chemicals in a correct ratio defined by the produced board grade. The grade also affects other handlings of the pulp. Stock preparation has a major influence on the board machine’s viability because it affects the quantity and quality of the board production. Pulp cannot be used in a board machine

coming straight from the mill. It requires slushing and other processing to create the best possible properties. Various solid and dilution mixtures are mixed, and the mix is processed in various handling components. Refined pulp, to which the necessary fillers, dyes, additives and other chemicals are added, can be called a stock. It is used to a create specific type of board in the board machine (Glossary of Papermaking Terms, 2016). The main processes in stock preparation are mixing, refining and screening. Mixing is done in agitators, which maintains high stock uniformity. Stock is refined in refiners where the refiner blades cut the fibers. This improve the board's strength and the smoothness of the surface. Unwanted particles are removed from the flow in screens. The removed parts are called rejects and the accepted parts are called accepts. (Paulapuro 2007, 165-168)

The board machine can be divided into four different stock and water systems with specific roles. The four systems are:

- Stock preparation which mechanically handles the pulp, ensuring that it is suitable for board machines;
- An approach flow system which comprises the area between the headbox feed pump and the headbox. Its main function is to move the stock to the board machine;
- A short circulation collects the water that is removed from the board machine's wet end and circulating it to diluting the thick stock flow before the headbox;
- A long circulation collects the removal waters from the short circulation and board machine. The collected water is then mainly used for stock dilution. (Paulapuro 2007, 142)

2.2 Headbox

The stock moves to the board machine through the headbox. The main function of the headbox is to apply the stock to the wire with a steady and regular distribution to the entire width of the machine. (Paulapuro 2007, 233)

2.3 Forming

After the headbox, the stock moves to the forming section, where a web is formed. The forming section can also be called the wire section. When it arrives to the forming section, the web's fiber consistency is 2-10 grams of fiber to 1 liter of water, which means that fiber content is 0,1 to 1,0 %. (Karlsson 2009, 14) The web lays on top of the forming fabric (also called the wire), which supports the carrying of the web through the wire section to the press section. The dewatering of the web is started in the wire section, which removes the water from the web mainly using a vacuum. (Paulapuro 2007, 247-248)

In the first paper machines, water was removed using the Fourdrinier method, in which water was removed using suction and gravity. The old Fourdrinier method is replaced with newer methods in modern board machines. Modern methods, which are mainly using suctioning, are more efficient in dewatering than older gravity-based methods. Newer machines use the twin wire method, which was invented in the 1950s and became more common in the 1970s. In the twin wire method, the web is formed and dewatered between two wires. This enables efficient two-sided dewatering compared to the older methods' one-sided dewatering. In addition to better dewatering, the twin wire former increases the quality and the structure of the board, because it protects the web from the air from both sides. This prevents it from easily mixing with the web. (Paulapuro 2007, 258-259; 277)

Suction in the forming section is executed with suction units. Specifically, the suctioning components are suction boxes or suction rolls. Typically, the last component of the forming section is the couch roll and all the components before it, are suction boxes. Suction is created with vacuum blowers that create negative pressure inside the suction units. The component then suctions the wire and web through gaps on its surface. The vacuum in the suction boxes is typically between 15-40 kPa and in the roll typically 40-80 kPa, but these vary according to the producing grade and machine design. (Paulapuro 2007, 255) The wire speed is typically between 100-2000 m/min but this also varies according to the grade and machine design to enable enough dewatering to occur. (Paulapuro 2007, 310) After the wire section's dewatering, the dry content of the web is typically 15-23 % (Karlsson 2009, 14).

2.4 Pressing

After forming, drying and handling of the stock is continued in the pressing section. The press is a wringer device that consists of loaded top and bottom rolls. The felt and wet web pass through the nip between the two rolls, where water is compressed out of the web into the felt. The contact point between the two rolls is called a nip. (Glossary of Papermaking Terms, 2016) To enhance water removal, rolls can be heated for increased evaporation. The roll's other function is to work as a carrier and supporter for the felt and the web. In addition to compressing, suction components are used in dewatering in the pressing section. (Paulapuro 2007, 344) After pressing section, the dry content of the web is typically 35-55 % (Karlsson 2009,14).

The performance of the pressing section is affected by the mechanical design, but it can also be affected by driving parameters. The machine speed affects the residence time of the web in the pressing section, which directly affects water removal. The nip loads can be changed, which means harder or softer compression. Temperature is also an important factor in the pressing section. A 10 ℃ increase in the pressing temperature results in approximately 1 % higher dry solids content after pressing, depending also on the produced grade. The reason for this is that water viscosity and surface tension decrease, and the web's fibers soften because of the increasing temperature. (Paulapuro 2007, 359-360)

In addition to the drying attributes, the pressing section affects to the quality of the end product. Compression in the pressing section affects the board's mechanical compaction. The pressing section also influences the distribution of the sheet thickness density. (Paulapuro 2009, 344)

2.5 Drying

The pressing section is followed by the drying section, which is the last dewatering section in the board machine. The drying section is usually divided into two sections: the pre- and after-dryers. These sections are divided with the sizer, meaning that the pre-dryer is before the sizer, and the after-dryer is after the sizer. (Karlsson 2009, 212-214)

Modern board machines' drying sections are multi-cylinder designs, in which drying occurs through contact with the cylinder. This is called contact drying. The dryer mainly consists of drying cylinders, which form multiple drying groups. Different drying groups are driven independently, and they each have their own felting. The popularity of the multi-cylinder dryer lies in its high energy efficiency compared to other solutions. Steam is used to heat the cylinders, and it is well suited to the board machine's energy infrastructure. The other benefits of the multi-cylinder design are its ability to transport web reliably and better smoothness in the end product. (Karlsson 2009, 80-81)

The multi-cylinder dryer's cylinders' diameters are many meters long. The shell thickness of the typical cylinder is 25-45 mm, but the thickness may be greater. The diameter is limited by the increasing peripheral speed, as the materials cannot withstand high speeds. The cylinder material is usually cast iron, but nodular graphite iron is also used. The benefit of using cast iron is its good heat conductivity, which is around 50 W/m K. This is significantly better than graphite iron's 30 W/m K. Nodular graphite iron's advantage compared to cast iron is its better strength properties (Karlsson 2009, 91). Drying occurs at the dryer section through evaporation. The drying cylinders are heated by steam for effective evaporation when the sheet passes over it. The used steam is typically at a low pressure, between 1 to 5 bar. It enters the cylinder by use of a steam switch. The steam pressure is lower near the wet end and higher at the after-dryer where dry solids content is higher, and evaporation does not happen as easily. Low-pressured steam would be the most cost-effective solution, but it leads to lower drying power. (Karlsson 2009, 115-116)

The drying section is covered with a hood. It is designed to ensuring optimal drying conditions and removal of moist air. (Glossary of Papermaking Terms, 2016) The fan removes the moist air from the hood ceiling and this air is utilized in heat recovery. The air's high moisture and temperature provide high thermal power to be recovered in heat recovery units. (Karlsson 2009, 441)

2.6 Sizing

Sizing consists of a processing component called a sizer, which is located between the pre- and the after-dryers. It typically consists of two rubber-covered rolls. The sizer adds size to the surface of the web. The size consists of rosin, gelatins, glues, starch or waxes.

This increases the board's water-resistant characteristics. (Glossary of the Papermaking Terms, 2016)

2.7 Calendering

The board's surface properties are improved in calendering, which is done after the drying section. All the necessary water is removed before the calender, dewatering is therefore unnecessary in the calender. In calendering, the board is pressed between two or more rolls. The mechanical work of the compressing affects the characteristics of the board surface. The main purpose in calendering is typically to lessen surfaces roughness. The process can also decrease the board's strength properties, making calendering a trade-off between positives and negatives. (Rautiainen 2009, 14-15) Calendering is typically done before the reel-up in-line at the board machine but it can also be done off-line (Glossary of Papermaking Terms, 2016).

Calenders can be divided into two main types: hard nip and soft nip calenders. The hard nip calender's rolls are polished metal. It is versatile, because it can be used for many different board grades. The hard nip calender consists of two or more hard rolls, which compress the sheet in the nip. Two rolls are used when the produced grades do not require a lot of calendering. More than two rolls must be used for the more challenging grades. The other main type is the soft nip calender. Its rolls are of composite material. Soft nip calenders have one or more soft-surfaced rolls. A soft surface creates less compression in the nip. This produces constant density in the produced board. The disadvantage of the soft nip calender is its inconsistent caliber, which means that the board's surface is not smooth. In contrast, the hard nip calender produces a consistent caliber but inconsistent density. (Rautiainen 2009, 19-22)

2.8 Reeling and winding

After calendering, the board is finished. In reeling, the complete board is wound into a big roll around the reel spool. The finished roll is called a parent-roll, and it is used for storage and transportation of the finished product. The roll's diameter is approximately close to its width, and the roll may weigh 120 000 kg. A good functioning of the reeling process enables high production rate for the machine. Good reeling operation consists of

an efficient turn-up sequence, which is the time when the full parent-roll is removed from the machine, and the new reel-spool starts. Reeling efficiency is measured in two different forms: material efficiency and time efficiency. Material efficiency is more important than time efficiency as it comprises 60-80 % of efficiency of reeling. Material efficiency considers the wasted materials and time efficiency consists of lost time in web breaks and shutdowns. (Rautiainen 2009, 192-194)

The parent rolls are unwound and then wound into smaller rolls, called customer-rolls. This process is called a winding. The rolls need to have certain and uniform characteristics for efficient handling. They need to have certain dimensions and straight edges, and they must be round and have certain hardness and structure. (Rautiainen 2009, 176)

3 DRYING SECTION HOOD AND VENTILATION

Water is removed from the web by evaporation in the drying section, which increases the air's humidity inside the hood. For a drying process to be working efficiently, the moisture must be removed from the hood. (Karlsson 2009, 438) Moist air is removed from the hood by the ventilation system, which is described in this chapter.

3.1 Description of the hood

The hood covers the drying section, and it makes the drying section environment more controllable. The hood consists of a closed hood, basement enclosure, exhaust and supply air equipment, air distribution devices and a heat recovery system. The hood's main functions are to ensure

- even drying for the whole width of the web
- better board quality by preventing contamination
- the process' independence from seasonal changes
- protection against corrosion
- better working conditions around the board machine
- better energy efficiency of the board machine (Villalobos, 1985)

Moist air flows inside the hood are illustrated in the figure 3.1, which shows that evaporation occurs at both the top and the bottom sides of the sheet. Moist air is moving towards the hood ceiling where it is removed through a false ceiling. Leakage air moves to the basement enclosure from outside of the hood.

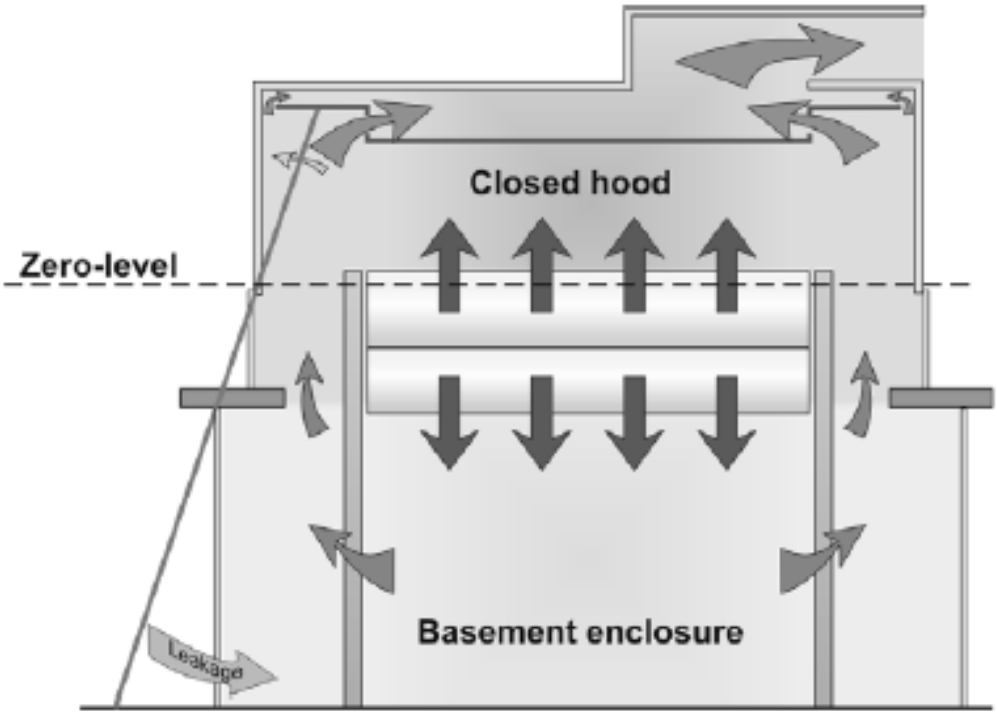

Figure 3.1. Air flows inside the hood (Valmet internal).

Water is evaporated from the sheet to the top and bottom sides. Because of the lower pressure above zero level, the air moves towards the hood's false ceiling. The purpose of the false ceiling is to ensure adequate control of the air flows, which stalls the condition of the hood. Moist air is removed from the ceiling via the exhaust ductwork to the heat recovery system and then discharged outside. Exhaust air is replaced by drier supply air. The difference between the amounts of exhaust and supply air is filled by leakage air. It typically covers 10-35 % of the exhaust air, which varies based on machine design. Air leaks to the basement enclosure because of the lower pressure of that section. Despite the required leakage, the hood must be air-tight and as well insulated as possible. A tight hood ensures efficient energy economy as warm and moist air is not lost outside the system and can be utilized in heat recovery. In addition, good insulation keeps the hood's inside wall surfaces warm, which prevents condensation. (Karlsson 2009, 442-445)

3.2 Important parameters in the ventilation

The drying section ventilation's function is to produce and sustain operating conditions that enhance the best possible drying process and minimize energy consumption.

According to Karlsson (2009), 8-10 % higher drying rates are achievable by optimizing the drying section ventilation. The most important operating parameters are exhaust air humidity, temperature, pressure zero level and the leakage air ratio. Typical values for hood parameters are presented in table 3.1. (Karlsson 2009, 450)

Table 3.1. Typical hood parameters (Karlsson 2009, 444)

	Typical value for the parameter
Typical exhaust air temperature	80-90 °C
Typical exhaust air humidity	160-180 g H_2O/kg d.a.
Dew point	60,8-62,8 °C
Typical leakage air ratio	10-35 %
Required exhaust air flow to remove 1 kg of water per second	6-7 kg d.a./s

3.2.1 **Humidity**

Water evaporation in the drying section causes the air inside the hood to be very humid. Hood humidity is typically referred as an exhaust air humidity as it is monitored because it transports the water out of the hood. Exhaust air humidity is typically displayed as absolute humidity, because it illustrates the real amount of water in the air. Absolute humidity's unit is g H_2O/kg dry air, which is a ratio between the masses of the water content of the air and dry air. The typical value for the humidity in modern hoods is 160-180 g H_2O/kg dry air, as presented in table 3.1. Older hood designs were only able to sustain lower humidities. (Karlsson 2009, 441) Relative humidity is not used, as it only demonstrates the amount of water compared to the saturation point.

High exhaust air humidity is preferred as humid air contains higher thermal power than drier air. This leads to higher recovered power in the heat recovery system. However, if the humidity is too high, water condenses on the hood's surfaces. Condensation occurs when the surface temperature is lower than the air's dew point. The dew point is the

temperature at which the air becomes saturated with water vapor. Table 3.1 shows that the typical dew point is 60,8-62,8 °C. The dew point is defined as a function of air humidity. If condensation occurs, condensed water will drain back to the web, leading to unnecessary increased moisture at the web. Condensation lowers the absolute humidity of the air, which also affects heat recovery with less power being recovered. (Karlsson 2009, 442-445)

Humidity is not uniform inside the hood. In some places the humidity is lower, and in some places, it is higher. Therefore, the hood must sustain higher humidity than the dimensioned humidity. Hood is typically designed conservatively fearing the condensation, because of lack of the exact knowledge on local air flows and humidities. Sufficiently working ventilation helps to prevent humidities that are too high locally, which may lead to condensation or an uneven moisture profile on the sheet. Sufficient humidity is especially needed near the sheet where evaporation occurs. Good humidity is achieved by importing the dry supply air to the pockets near the sheet using blow boxes. This enables high evaporation rate from the sheet. In contrast, inefficient ventilation causes the humidity to be gathering into the drying pockets, which negatively influences on the drying rate. Pocket humidity is 150-300 g H_2O/kg d.a. in typical board machines, depending on used steam pressure. (Karlsson 2009, 445-450)

3.2.2 **Leakage air ratio**

As its name suggests, the leakage air ratio presents the share of leakage air in incoming air flows. The leakage air ratio is typically around 10-35 %, as presented in table 3.1. This means that exhaust air amount is greater than supply air amount. A 10-35 % air deficit is filled by leakage air from outside of the hood. The leakage air ratio is used to adjust the pressure zero level. In some designs, recirculation air is used in the ventilation system. This means taking air from the hood and combining it with the supply air. Recirculation air does not affect the leakage air ratio. (Karlsson 2009, 451-452)

In addition to replacing the exhaust air, the supply air's direction also affects the drying section. As noted previously, supply air is directed to near the sheet for lowering the local humidity for efficient drying rate. Supply air is also needed in the basement enclosure where it prevents the possible condensation otherwise caused by leakage air. Supply air

is directed to certain other areas of the hood as well to sustain a constant air flow, thus preventing too high local humidities. (Karlsson 2009, 451-452)

3.2.3 **Pressure zero level**

Removal of the exhaust air from the hood is based on the "chimney effect", where the exhaust rises to the hood ceiling. This is presented in figure 3.1. This phenomenon occurs because the density of the warm and moist air in the hood is lower than the density of the air outside the hood at the same height. Because of the lower density inside the hood, the pressure decrease from the base floor is smaller than the decrease is outside the hood. The zero level is at the level where pressure inside the hood is equivalent to the pressure outside the hood. This level is normally 2-2,5 meters above the operation floor level. Pressure differences are relatively small, around 0-30 Pa, but they are sufficient to be moving the air. (Karlsson 2009, 442-445)

The pressure zero level is adjusted by changing the leakage air ratio. A high amount of supply air lowers the zero level. When the zero level is too low, moist air flows from the hood to the machine hall through openings that are above the zero level. This affects energy efficiency, as less humid air flows through the heat recovery, and there is also a possible risk for condensation in the openings or exterior of the hood. (Karlsson 2009, 442-445)

4 HEAT RECOVERY SYSTEM OF BOARD MACHINE

This chapter covers the functioning of heat recovery in the board machine environment. The objective of the heat recovery system is to economically decrease primary energy consumption in the board machine by utilizing the drying section's secondary energy. The heat recovery system is used to capture and utilize the thermal power of the exhaust air that would otherwise be lost to outside the system. This enhances the board machine's overall energy efficiency, thus being important factor in cost reduction. Ideally, all the energy used for drying should be possible to recover, but the recovering efficiency is lower in practice. In colder areas, for example in Scandinavia, heat recovery can save more than 50 % of the overall primary energy consumption in the winter months, when heating requirements are high. Monetary savings are significant given that energy consumption constitutes up to 10 % of the costs in the board making industry. (Sivill et al., 2005) A newsprint machine drying section's energy streams are presented as the Sankey diagram in figure 4.1. The diagram demonstrates the importance of the heat recovery system as 63 % of the exhaust power is recovered. Boardmaking is an energy intensive industry, where small percentage differences in energy consumption produce a significant savings or costs. In the board machine, recovery efficiency is typically slightly lower than presented in figure. In addition, it is difficult to compare the amounts of recovered heat between different machines. A comparing is difficult even between different production rates for one machine. This is because the whole boardmaking process must considered in terms of energy consumption, not just a heat recovery system. (Karlsson 2009, 454-459)

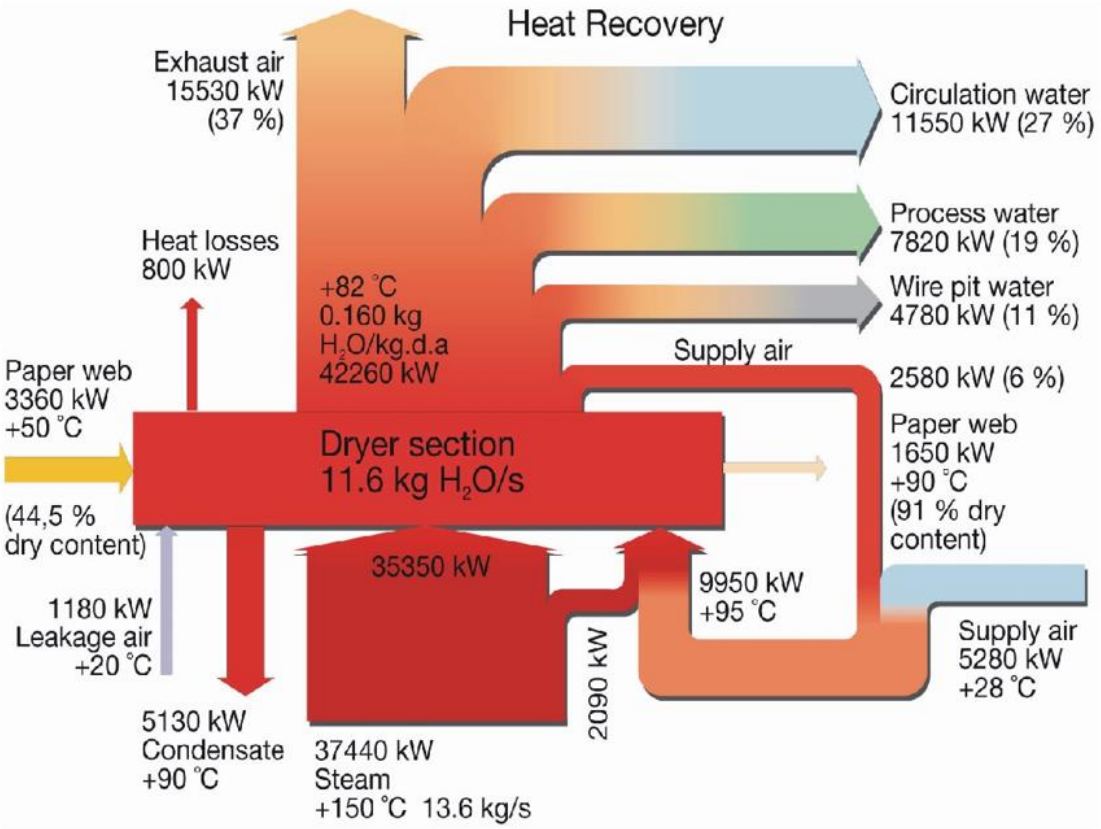

Figure 4.1. Sankey diagram of the drying section's energy streams (Valmet internal)

4.1 Description of heat recovery network

The hood's heat recovery system consists of a network of multiple heat recovery units. Heat exchangers are used to heat the air and water streams in their corresponding heat exchangers. (Sivill et al., 2005) Heat is recovered from the hood exhaust air. Typically, a board machine's heat exchangers are used to heat one to three different air or water streams, depending on the machine design. The heated streams are:

1. Hood supply air
2. White water or wire pit water
3. Machine hall ventilation system's circulation water

The order of heating units is determined by the different streams' heating and final temperature demands. In a modern board machines, the hood's supply air is always heated in a heat exchanger and this exchanger is typically located first, because the supply air has the highest final temperature demand at over 90 °C. The supply air is typically heated

to 55-65 °C in the conventional heat recovery unit (CHR), and the rest is heated in a steam coil after the CHR. This is followed by white water, process water and circulation water, typically in that order. The CHR is followed by either the machine hall's circulation heating aqua heat recovery unit (AHR), or a white or wire pit water heating AHR, depending on the design. Circulation water is heated before the water if the machine hall's heating requirement is high, as is typically the case when the machine is located in a colder climate. The white or wire pit water unit could be before the circulation water if it is considered more valuable. (Karlsson 2009, 466-467) The heat recovery system usually covers all the heating demand. Exceptions to this rule are the supply air, which is heated to the final temperature with steam coils, and machine hall ventilation in winter, when its heating demand is high. (Kilponen, 2002)

The drying section heat recovery system typically consists of multiple heat recovery unit stacks. One stack includes multiple heat exchangers that can be set in parallel or in a series. The advantage of multiple stacks is that they enable the use of multiple smaller exchangers compared to one big unit. The space requirements for multiple small stacks are smaller than for one big stack. Another advantage of multiple stacks is that they can be located in different areas, thus requiring less ductworking and transportation of the exhaust air. (Karlsson 2009, 470)

In addition to the heat exchangers, the heat recovery system needs a cleaning system, which keeps the heat transfer surfaces clean. Cleaning is an important factor in heat recovery, as plugging negatively affects the heat transfer. Fresh water and water-glycol circuits are less prone to plugging, thus the cleaning is not as important as cleaning of white water and wire pit circuits. These waters contain fibers, fillers and residues, which predispose to the deposits in the heat exchanger channels. (Karlsson 2009, 468-469) Cleaning showers are located above the heat exchangers. They clean the exchangers by spraying water on them at regular intervals for only short periods. A typical cleaning cycle might be 1 minute of cleaning every hour. (Karlsson 2009, 475)

Modern board machines are combining CHR and AHR units in the same heat recovery tower, which is called a CAHR tower. Older machines' towers are typically consisted of only either CHR or AHR units. (Karlsson 2009, 470-472) A typical board machine's

layout for the heat recovery network is presented in the figure 4.2. The machine presented in figure consists of one CHR unit and two AHR units.

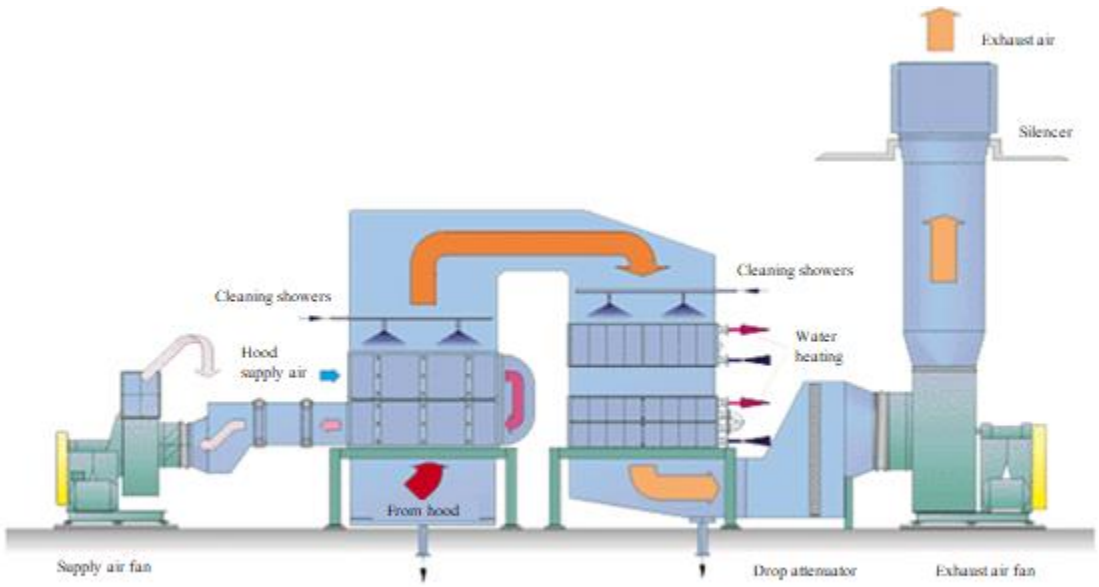

Figure 4.2. Typical layout of the heat recovery network in the board machine. This system layout is called a CAHR tower. (KnowPap)

4.2 Typical heat recovery units

The heat recovery network typically consists of two types of heat recovery units, CHR and AHR. Other types of heat recovery equipment can be used in board machines, but they are very rare in modern machines that are constructed after the 1980s (Kilponen, 2002). Such units are, for example, heating coils that are used to transfer heat from the water flow to the air flow and scrubbers where the emitting and absorbing flows are in direct contact with each other (Karlsson 2009, 469). The commonly used heat exchangers, the CHR and AHR units, are explained in more detail below.

4.2.1 Conventional heat recovery unit

A CHR is an air-to-air heat exchanger, which is used to exchange heat from the exhaust air flow to the supply air flow. The heat exchanger consists of an average of one hundred plates, joined in at their edges. The plates' dimensions vary from one meter to a few

meters, and they are made from stainless steel. There is a 10-30 mm space between the plates where the air flows. Every other slot between plates forms a duct for heat emitting exhaust air and every other slot is for heat absorbing supply air. Heat emitting and absorbing flows are not in direct contact with each other, meaning the heating occurs through the heating surface. Heat transfer from the exhaust air to the heating surface occurs partly by convection and partly by condensation. This depends on the exhaust air humidity and the supply air temperature. The emitting side of the flow is heated by convection. According to Karlsson, the heat transfer coefficient ratio between the exhaust and supply air side is 8:1. (Karlsson 2009, 467-468) The construction of a conventional heat recovery unit is presented in figure 4.3. In the figure, exhaust air flows through the heat exchanger vertically and supply air flows horizontally.

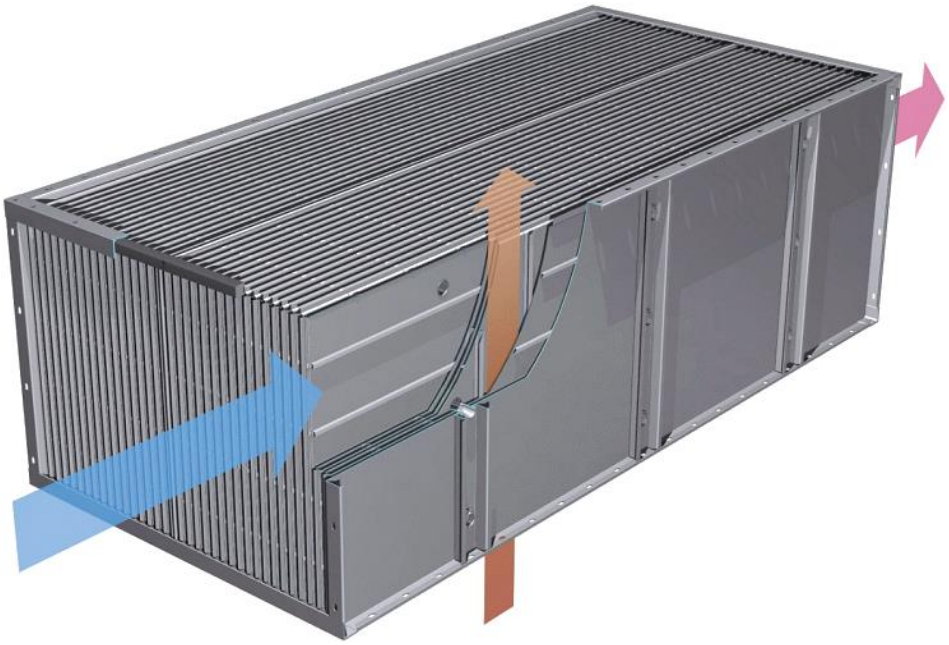

Figure 4.3. Conventional heat recovery unit (Valmet internal).

4.2.2 **Aqua heat recovery unit**

An AHR is an air-to-water heat exchanger, which is used to exchange heat from the exhaust air flow to a water flow. The heat exchanger consists of an average of one hundred elements that are close to each other, side by side on the water side. The elements are on top of each other in two rows. Water is flowing on the upper row. The heat emitting and absorbing flows are not in direct contact with each other, meaning that the heating occurs

through the heating surface. This is advantageous because then moist air does not contaminate the water with fibers, filler and other impurities. Heat transfers from the exhaust air mainly by convection to the heating surface, which then heats the absorbing flow by condensation. Heat exchange is more efficient on the water side, and the heat transfer coefficient ratio between the air and water sides is 1:8. (Karlsson 2009, 468-469) The construction of the aqua heat recovery units is presented in figure 4.4. In the figure, the exhaust air flows through the heat exchanger vertically, and the heat absorbing water horizontally making a U-turn inside the exchanger.

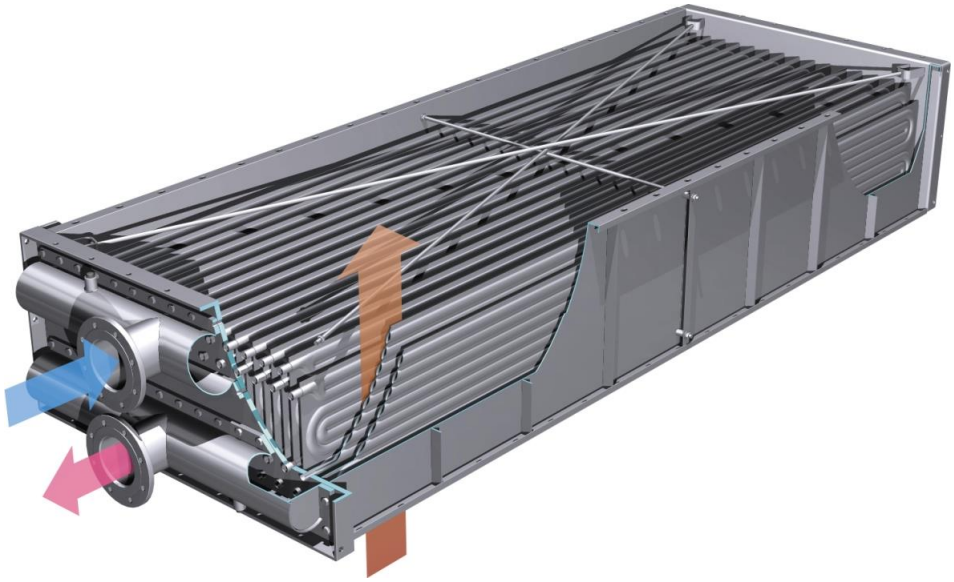

Figure 4.4. Aqua heat recovery unit (Valmet internal).

4.3 Optimization of heat recovery

Heat recovery is a complex process to optimize. The main objective for heat recovery is to lower the board machine's primary energy consumption. The frame of reference for lowering energy consumption is the entire boardmaking process, which means that the range of the examined scope is wide. This means that heat recovery cannot be optimized by itself, but the overall energy consumption of the boardmaking process must be optimized. (Karlsson 2009, 459) The heat recovery process is unpredictable because of the connections between multiple heat exchangers, thus increasing the difficulty of optimization. Change in one stream affects the whole process, making the designing of the heat recovery system difficult. (Kilponen, 2002)

Investment costs, processing costs, heating demands, heating performance and space requirements must be accounted for when designing the system. Large exchanger surfaces increase investment costs, but more efficient heat recovery saves money. Whereas high flow velocity enables smaller heating surfaces, it creates bigger pressure losses, which increase operational costs. The heat recovery system must be designed as a compromise between several aspects. (Karlsson 2009, 474) In addition, the system must always be designed considering the special needs of a particular situation. For example, energy prices are different for different board machines, and the prices vary continuously. Another challenge in the designing is the constantly changing circumstances. Changing board machine's operation parameters and seasonal weather changes challenge the performance of heat recovery. The machine hall ventilation's and process water's heating demands depend on the outside air temperature. The hood's supply air's and white water's heating demands remain constant, independent of the outside weather changes. (Karlsson 2009, 464)

Operational optimization is mainly done by changing the ventilation parameters that are presented in chapter 3.2, which are the humidity, the leakage air ratio and the pressure zero level. Increasing humidity decreases specific energy consumption, because less supply air is needed, which decreases the heating need. In addition to decreasing the heating need, higher humidity increases the condensation amount in heat recovery. This means higher heat recovery efficiency. Less air flow needs less power from the fan, which decreases electricity consumption. Smaller air flows require smaller ducts, fans and heat exchangers, which decrease costs and space requirements. Higher humidity also causes unwanted characteristics in heat recovery. Higher humidity may negatively affect the evaporation rate, which causes higher costs, because higher steam pressure is needed. Decreased evaporation rates can be avoided by good pocket ventilation, which keeps the pocket humidity sufficiently low. Increased steam pressures also have positive affects as they increase the hood's temperature, which decreases the risk of unwanted condensation. The leakage air ratio also affects the performance of the heat recovery system. If heat recovery alone is considered, the ratio must be as low as possible. In practice, the pressure zero level limits the ratio, and the hood must be able to handle a higher dew point. A low ratio means that the leakage air amount is low. Leakage air, which is colder than supply

air, increases specific energy consumption and it also predisposes the hood to condensation. (Karlsson 2009, 459-461)

5 MODELLING OF HEAT RECOVERY SYSTEM

Modelling of the board machine's heat recovery system is presented in this chapter. This includes an explanation of the heat transfer equations and introduces the created MATLAB models. The models are written in MATLAB and the codes are utilized in Simulink to creating a block library for heat recovery. In addition, a conceptual theory for a digital twin is discussed as the base idea for the model.

5.1 Heat transfer calculations

The basic heat transfer calculation methods are presented in this chapter. Equations are presented with necessary explanations and the meanings of the important parameters. Valmet's heat recovery system condition monitoring method is presented after the presentation of the heat transfer equations.

Convective heat transfer is calculated by multiplying heat transfer coefficient by the difference between the temperature of the surface and the temperature of the surrounding space. This equation is presented in equation 1. (Ghoshdastidar 2012, 4)

$$q = h(T_s - T_\infty) \tag{1}$$

where q convective heat transfer flux [W/m^2],

h convection heat transfer coefficient [W/m^2 K],

T_s surface temperature [K],

T_∞ surrounding temperature [K].

The Reynolds number is a dimensionless number that describes flow behavior. A low value suggests the flow is laminar and a high value suggests the flow is a turbulent. The Reynolds number can be calculated using equation 2. (Incropera et al. 2016, 390)

$$Re = \frac{\rho v L}{\mu} \tag{2}$$

where Re Reynolds number [-],

ρ density [kg/m^3],

v flow velocity [m/s],

L characteristic length [m],

μ viscosity [Pa s].

The Prandtl number is another dimensionless number that describes a flow behavior. It is the ratio between momentum and thermal diffusivity. The Prandtl number is calculated as (Incropera et al. 2016, 409)

$$Pr = \frac{c_p \mu}{\lambda} \quad (3)$$

where Pr Prandtl number [-],

c_p specific heat capacity [J/kg K],

λ thermal conductivity [W/m K].

The third important dimensionless number is the Nusselt number, which describes the ratio between conductive and convective heat transfer at the fluid boundary level. The Nusselt number equation can be calculated as presented in equation 4. (Incropera et al. 2016, 409)

$$Nu = \frac{hL}{\lambda} \quad (4)$$

where Nu Nusselt number [-].

The fluid-mix viscosity, which consists of two separate fluids, can be calculated with empirical equation 5. An empirical equation means that the equation is obtained by experimentation. (Ryti et al. 1981, 368)

$$\mu = \frac{\mu_1}{1+\phi_{12}\frac{\gamma_1}{\gamma_2}} + \frac{\mu_2}{1+\phi_{21}\frac{\gamma_2}{\gamma_1}} \quad (5)$$

where μ_1 viscosity, fluid 1 [Pa s],

μ_2 viscosity, fluid 2 [Pa s],

γ_1 mole fraction [-],

γ_2 mole fraction [-].

An empirical equation for the dry air viscosity is presented in equation 6. For the equation to be relevant, the pressure is assumed to be 1 bar. (Ryti et al. 1975, 746)

$$\mu_{d,a} = \frac{1{,}458 \cdot 10^{-6} \cdot \sqrt{T}}{1+\frac{110{,}4}{T}} \quad (6)$$

where $\mu_{d,a}$ viscosity for dry air [Pa s].

Equation 7 presents the corresponding empirical model for the viscosity of the vapor. In addition to the assumption that the pressure is 1 bar, the temperature must be under 800 °C. This assumption applies well to the heat recovery system of the hood, making the equation viable to use. (Ryti et al. 1975, 746)

$$\mu_{vap} = 0{,}0361T - 1{,}02 \cdot 10^{-6} \quad (7)$$

where μ_{vap} viscosity for vapor [Pa s].

ϕ_{ij} is utilized in equation 5. It is calculated using equation 8. (Kilponen, 2002)

$$\phi_{ij} = \frac{\left(1+\sqrt{\frac{\mu_i}{\mu_j}}\sqrt{\frac{M_j}{M_i}}\right)^2}{\sqrt{1+\frac{M_i}{M_j}}\sqrt{8}} \quad (8)$$

where M molecular mass [g/mol].

Thermal conductivity can be calculated similarly as the viscosity is calculated in equation 5. This is presented in equation 9, which is based on the Wassilijewa-Saxena-Mason rule (Ryti et al. 1981, 368).

$$\lambda = \frac{\lambda_1}{1+\phi_{12}\frac{\gamma_1}{\gamma_2}} + \frac{\lambda_2}{1+\phi_{21}\frac{\gamma_2}{\gamma_1}} \quad (9)$$

Dry air thermal conductivity can be calculated with empirical equation 10. The air pressure is assumed to be 1 bar. (Ryti et al. 1975, 755)

$$\lambda_{\mathrm{d,a}} = \frac{2{,}646\sqrt{T}}{1+\frac{245{,}4}{T}\cdot 10^{-\frac{12}{T}}} \cdot 10^{-3} \tag{10}$$

where $\lambda_{\mathrm{d,a}}$ thermal conductivity of dry air [W/m K].

In the case of vapor, thermal conductivity is calculated using a different equation. It can be calculated using empirical equation 11. (Ryti et al. 1975, 755)

$$\lambda_{\mathrm{vap}} = \left(\frac{6{,}471\sqrt{T}}{1+\frac{1737{,}3}{T}\cdot 10^{-\frac{12}{T}}} + 4{,}59 \cdot \left(10^{9{,}218\cdot p\cdot\left(\frac{100}{T}\right)^4} - 1 \right) \right) \cdot 10^{-3} \tag{11}$$

where λ_{vap} thermal conductivity of vapor [W/m K].

5.1.1 **Convection**

The general form of the Nusselt number equation is presented in equation 12. Coefficients C, m and n vary based on geometry and flow characteristics. The model is created based on equations where the flow characteristic is assumed to be an internal flow in a noncircular tube. (Incropera et al. 2016, 401)

$$Nu = C{Re_{\mathrm{L}}}^{m} Pr^{n} \tag{12}$$

where C coefficient [-],

m coefficient [-],

n coefficient [-].

The hydraulic diameter can be calculated using equation 13. It is utilized in calculations of the Nusselt and Reynolds numbers. (Ghoshdastidar 2012, 278)

$$D_{\mathrm{h}} = \frac{4A_{\mathrm{c}}}{P} \tag{13}$$

where D_{h} hydraulic diameter [m],

A_c cross-sectional area [m^2],

P wetted perimeter [m].

Nusselt number correlations differ based on whether the flow is laminar or turbulent. If the Reynolds number is under 2300, the flow is treated as laminar. In a laminar flow and fully developed conditions, the Nusselt number is calculated as shown in equation 14. (Yendler, 1994)

$$Nu_D = Nu_0 + \frac{0{,}0677\left(PrRe\frac{D_h}{L}\right)^{1,33}}{1+0{,}1Pr\left(Re\frac{D_h}{L}\right)^{0.83}} \quad (14)$$

where Nu_0 theoretical Nusselt number [-].

The theoretical Nusselt number Nu_0 can be estimated to be 4,36 in the laminar flow case. In the case of a turbulent flow, when the Reynolds number exceeds 2300, the Nusselt number is calculated with the correlation shown in equation 15. (Yendler, 1994)

$$Nu_D = 0{,}0235\left(Re_D{}^{0,8} - 230\right)(1{,}8Pr^{0,3} - 0{,}8)\left(1 + \left(\frac{D_h}{L}\right)^{0,66}\right) \quad (15)$$

5.1.2 **Heat transfer rate**

The method for calculating the heat transfer rate is dependent on the heat transfer method. In the hood's heat recovery system, the heat transfers by convection or condensation. The calculations are simpler in the case of convection. The heat transfer rate in the convection between streams 1 and 2 can be calculated using equation 16. (Ghoshdastidar 2012, 34)

$$Q = UA(T_1 - T_2) \quad (16)$$

where Q heat transfer rate [W],

U overall heat transfer coefficient [W/m^2K].

The overall heat transfer coefficient can be calculated using the convection coefficients of both streams, and the thermal conductivity and thickness of the surface. The equation is formed as (Ghoshdastidar 2012, 33)

$$U = \frac{1}{h_1 + \frac{\lambda_s}{s} + h_2} \quad (17)$$

where s thickness of the heat transfer surface [mm].

In the case of condensation, the calculation is more complicated. In condensation, vapor condenses onto the surface in liquid form. Condensation occurs when the surface temperature is lower than the dew point of the air. Because of the form change, latent heat must be considered. When condensation occurs, the heat transfer rate is calculated as presented in equation 18 (Ghoshdastidar 2012, 383)

$$Q = h_1 A_1 (T_1 - T_s) + \dot{m}_c A_1 l \quad (18)$$

where T_s surface temperature [K],

$\dot{m}_c$ flow rate of condensation [kg/s],

l latent heat [J/kg].

Substitutions can be made where equation 18 can be formed into a simpler equation. A simpler version of the condensation heat transfer rate is presented in equation 19 (Kilponen, 2002)

$$Q = \frac{A_2}{\frac{s}{\lambda_s} + \frac{1}{h_s}} (T_s - T_2) \quad (19)$$

The flow rate of the condensation for the calculation of the heat transfer rate can be solved using equation 20. (Kilponen, 2002)

$$\dot{m}_c = M \frac{p}{RT} k ln \left(\frac{p - p_{vap}(T_s)}{p - p_{vap}} \right) \quad (20)$$

where R universal gas constant [J/mol K],

k mass transfer coefficient [m/s],

p pressure [Pa],

$p_{vap}(T_s)$ pressure of vapor in surface temperature [Pa],

p_{vap} pressure of vapor [Pa].

Equation 18 and 19 can be merged together and when equation 20 is substituted into that, equation 21 is got. It can be used for solving surface temperature iteratively.

$$h_1(T_1 - T_\mathrm{s}) + lM\frac{p}{RT_{\mathrm{sat}}}kln\left(\frac{p-p_{\mathrm{vap}}(T_\mathrm{s})}{p-p_{\mathrm{vap}}}\right) - \frac{A_2}{A_1}\frac{(T_\mathrm{s}-T_2)}{\frac{s}{\lambda_S}+\frac{1}{h_2}} = 0 \quad (21)$$

The pressure of the vapor can be calculated when the overall pressure and absolute humidity are known. This is presented in equation 22.

$$p_{\mathrm{vap}} = \frac{x}{x+0{,}622}p \quad (22)$$

where x absolute humidity [g H_2O/kg d.a.].

An estimate can be made for the pressure of the saturated vapor at the surface temperature. It is calculated as presented in equation 23. (Kilponen, 2002)

$$p_{\mathrm{vap}}(T_\mathrm{s}) = p \cdot e^{\frac{11{,}78(T_\mathrm{s}-372{,}79)}{T_\mathrm{s}-43{,}15}} \quad (23)$$

The mass transfer coefficient is needed when calculating the condensation flow rate. It is calculated using equation 24. 0,33 is used as a factor *n* for the air. (Ghoshdastidar 2012, 508)

$$k = \frac{h_1}{\rho_1 c_{p1}}Le_1{}^{(1-n)} \quad (24)$$

where Le Lewis number [-].

The Lewis number is a dimensionless number, which describes the ratio between thermal and mass diffusivities. The equation for the Lewis number is typically presented as in equation 25, but it can also be calculated as shown in equation 26. (Incropera et al. 2016, 409)

$$Le = \frac{h}{D_{\mathrm{AB}}} \quad (25)$$

where D_{AB} mass diffusion coefficient between components A and B [-].

$$Le = \frac{\lambda}{D_{\mathrm{AB}} c_p \mu^2} \tag{26}$$

A correlation for calculating the binary mass diffusion coefficient was presented in a study by Fuller et al. (1966). Equation is presented in the equation 27 (Fuller et al. 1966, 18-27)

$$D_{\mathrm{AB}} = 0{,}0101 \frac{T^{1{,}75}\left(\frac{1}{M_{\mathrm{A}}}+\frac{1}{M_{\mathrm{B}}}\right)^{0{,}5}}{p\left((\sum v_{\mathrm{A}})^{\frac{1}{3}}+(\sum v_{\mathrm{B}})^{\frac{1}{3}}\right)^2} \tag{27}$$

5.1.3 **Condition monitoring based on heat transfer modelling**

Valmet has developed a heat recovery efficiency coefficient value, which illustrates the efficiency of the heat recovery while considering heating needs. This provides a method for comparing the efficiency of a heat recovery in different conditions. The equation for the heat recovery efficiency coefficient is presented in equation 28.

$$EFF_{\mathrm{rec}} = \frac{Q_{\mathrm{rec}}}{Q_{\mathrm{pw}}+Q_{\mathrm{mh}}+Q_{\mathrm{sup}}} \frac{\dot{m}_{\mathrm{ev,dim}}}{\dot{m}_{\mathrm{ev}}} \tag{28}$$

where EFF_{rec} heat recovery efficiency coefficient [-],

Q_{rec} recovered heat [W],

Q_{pw} heating demand for process water [W],

Q_{mh} heating demand for machine hall [W],

Q_{sup} heating demand for supply air [W],

$\dot{m}_{\mathrm{ev,dim}}$ dimensioned evaporated water flow [kg/s],

$\dot{m}_{\mathrm{ev}}$ evaporated water flow [kg/s].

The same equation can also be calculated as presented in equation 29. The equation is similar to equation 28, but without dimensioned evaporated water flow, which is a machine-specific value. This factor can be omitted from the equation, especially when

comparing the same heat recovery units at different times. The efficiency coefficient can be multiplied by this factor later to obtain the equation's former format.

$$EFF_{\mathrm{rec}} = \frac{Q_{\mathrm{rec}}}{Q_{\mathrm{pw}}+Q_{\mathrm{mh}}+Q_{\mathrm{sup}}} \frac{1}{\dot{m}_{\mathrm{ev}}} \quad (29)$$

Certain measurements are needed to calculate the efficiency coefficient reliably. The most important parameters are the streams' flow rates, temperatures and the exhaust air's humidity. Without these measurements, the values must be approximated, which reduces the calculation's accuracy.

5.2 Simulink model for heat recovery system

Simulink is a built-in tool in MATLAB, which is designed for building models for dynamic systems. A typical Simulink model consists of connected block diagrams. The standard Simulink library offers multiple blocks for different purposes, and many of these blocks can be modified to suit specific needs. (Colgren 2005, 153) The Simulink models in this thesis are created for CHR and AHR units. The modelling is based on the heat transfer equations that are presented in a chapter 5.1. The model is different for both heat recovery units because of their different geometries and operation principles. The CHR and AHR models are presented in chapters 5.2.1 and 5.2.2.

5.2.1 CHR model

The model models the behavior of the heat recovery in a CHR unit. It calculates the temperatures and humidities of the exhaust and supply air flows iteratively in the grid. In addition to the temperatures and humidities, the model calculates the recovered power from the exhaust air to the supply air. The model needs the following data as an input:

- Supply air flow rate, inlet temperature and inlet humidity
- Exhaust air flow rate, inlet temperature and inlet humidity
- Plate slits on exhaust and supply air side
- The height and length of the heat recovery unit
- The width of the unit
- The number of heat transfer plates

The model models the heat exchange at two different stages, which corresponds to the two-level structure of the CHR unit. The temperatures and humidities are modelled in the grid, which improves the model's accuracy. The calculation grid is presented in a figure 5.1. The used grid consists of 30 nodes for the supply air direction and 30 nodes for the exhaust air direction, meaning that the grid contains 900 nodes. The dimensions are based on a compromise between the calculation time and results accuracy. The selection is based on the graph presented in appendix I, which visualizes how the number of nodes influences on the calculation time and its accuracy. Calculation using a 30x30 grid takes approximately 15 seconds and provides sufficiently accurate results. It is important to save processing capacity when computing in a cloud service in real-time. The supply air is calculated in a direction of the x-axis and the exhaust air is calculated in a direction of the y-axis.

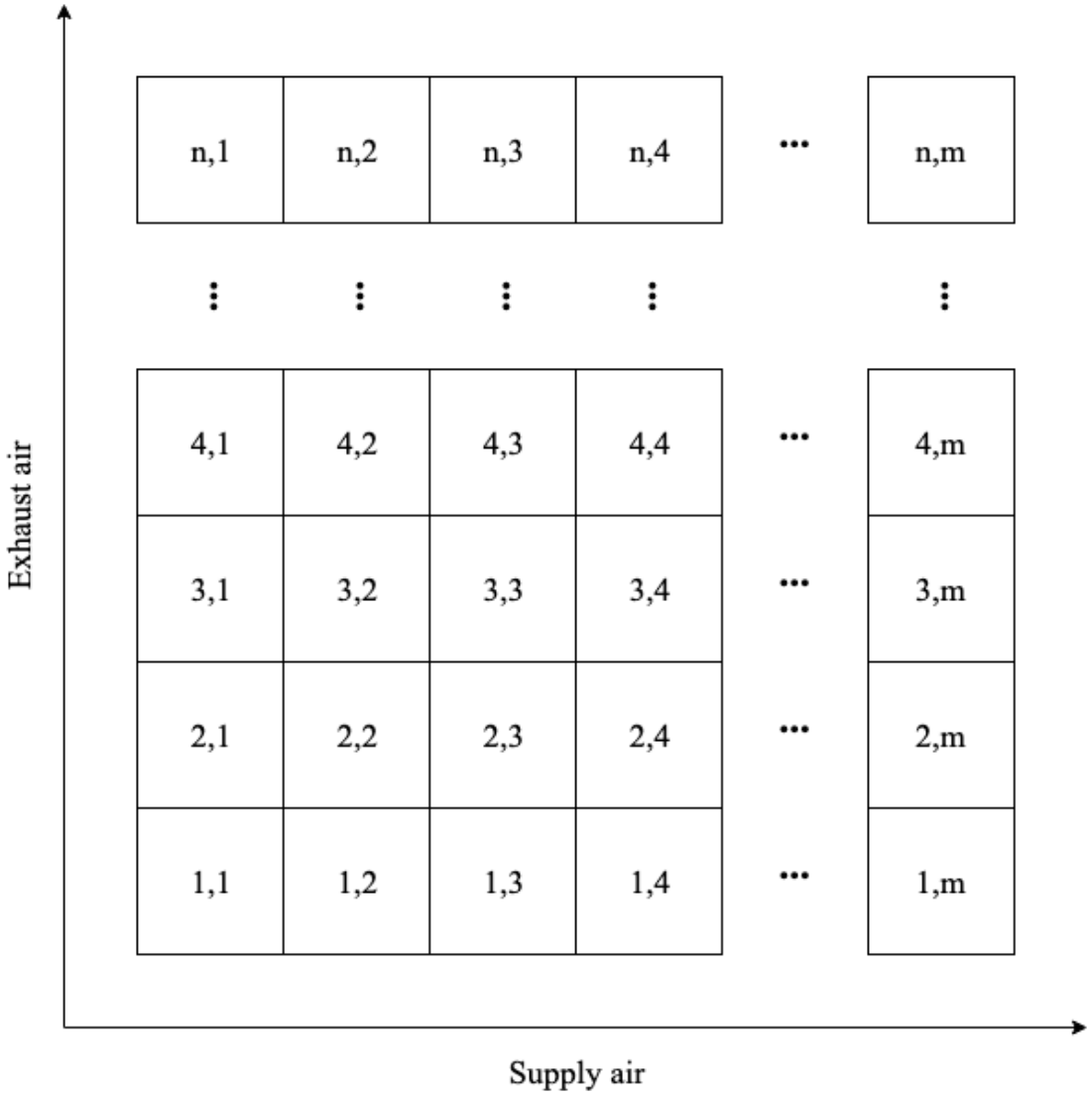

Figure 5.1. Calculation grid for the CHR model.

The model iterates the calculation until the results are converged. The iteration's starting point is to guess the supply air temperature at the U-turn, which is between the upper and lower sections. The initial guess is estimated to be the average of supply air inlet temperature and the exhaust air inlet temperature, which are entered as input data. The temperature in the U-turn is obtained as a result from the model, which then serves as a new initial guess at the next iteration loop. The iteration stops when the result and the last initial guess are converged. The structure of the CHR model is presented in a figure 5.2.

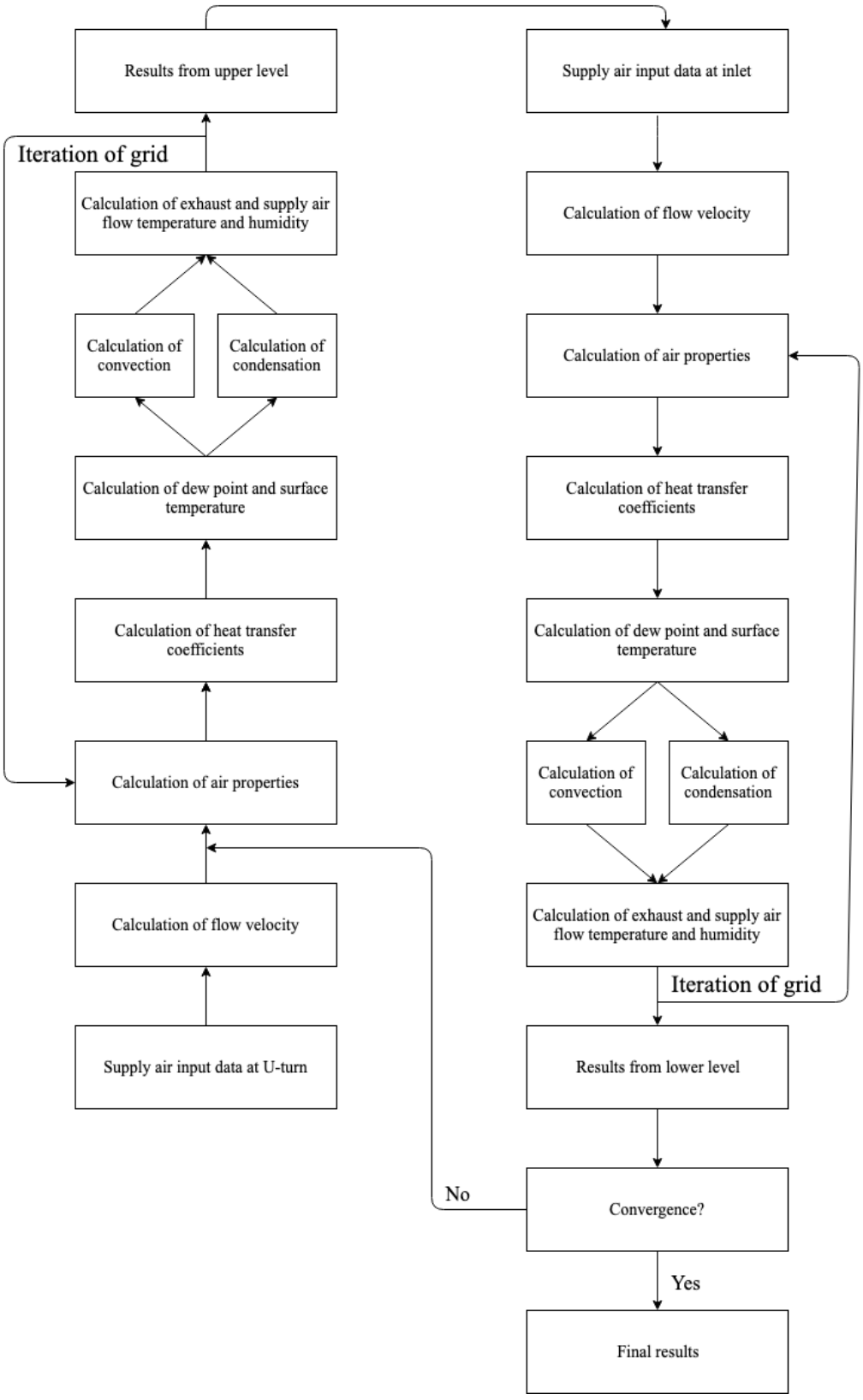

Figure 5.2. Structure of the heat transfer model for the CHR unit.

5.2.2 **AHR model**

The model models the behavior of the heat recovery in an AHR unit. It calculates the water temperature and the temperature and humidity of the exhaust air flow iteratively in the grid. In addition to the temperatures and air humidity, the model calculates the recovered power from the exhaust air to the water. The model needs the following data as an input:

- The water flow rate, glycol content and inlet temperature
- The exhaust air flow rate, temperature and humidity at inlet
- The unit type, which is selected from a pre-determined list of standard units

The temperatures and air humidity are modelled in a grid, which improves the model's accuracy. The grid size is dependent on the modelled unit type, but the size is a compromise between time consumption and modelling accuracy. The time consumed in AHR modelling is minimal compared to the CHR model, which enables an emphasis on greater accuracy. The calculation grid is presented in a figure 5.3.

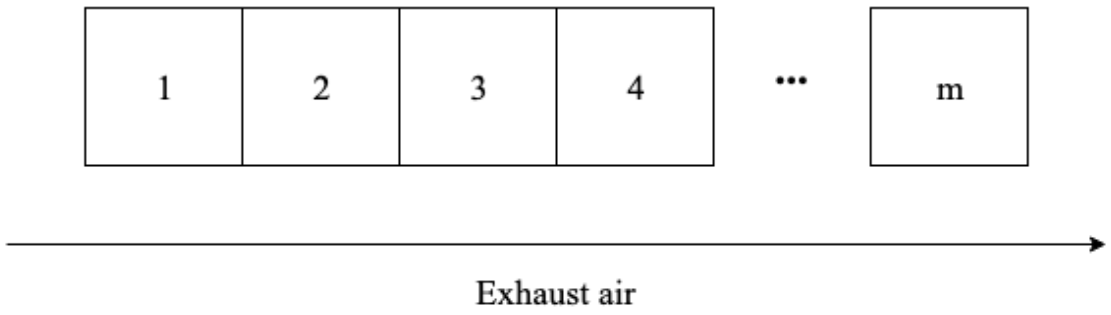

Figure 5.3. Calculation grid for the AHR model.

The model iterates the calculation until the results are converged. The iteration's starting point is to guess the water outlet temperature. The water outlet temperature is obtained as a result from the model, which then serves as a new initial guess at the next iteration loop. The iteration stops when the result and the last initial guess are converged. The structure of the AHR model is presented in a figure 5.4.

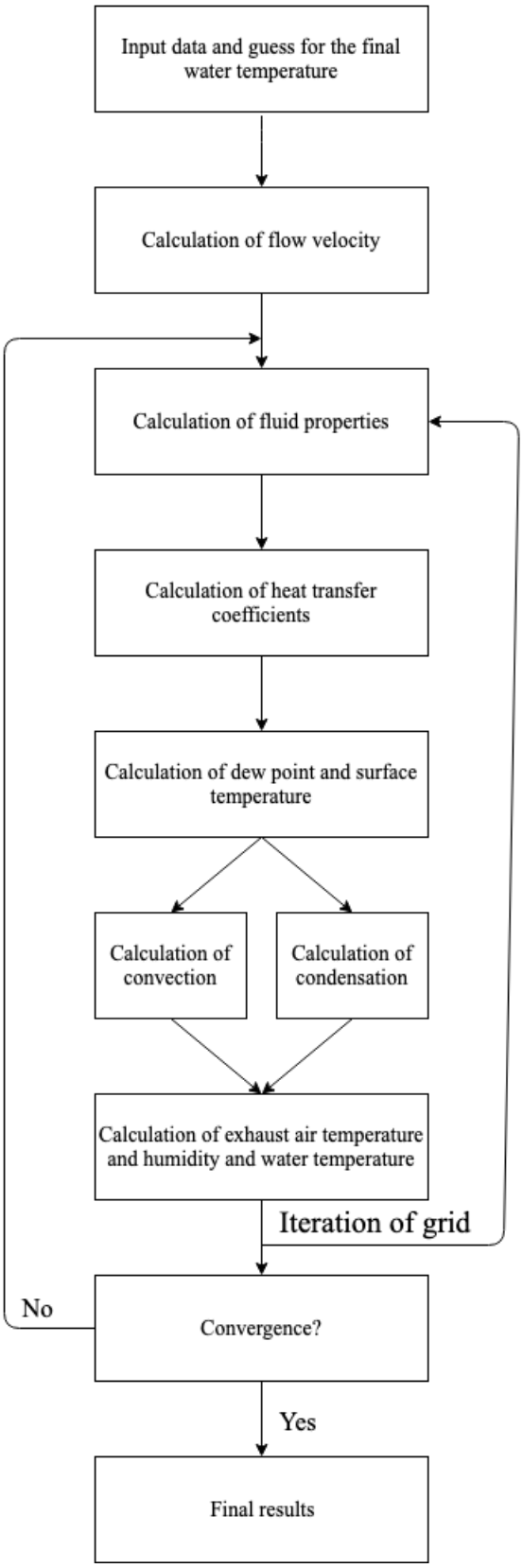

Figure 5.4. Structure of the heat transfer model for the AHR unit.

5.3 Digital Twin

The concept of a digital twin was discussed for the first time in 2003, but it did not gain popularity until the 2010s. The development of sensor and cloud technologies has decreased costs and increased the utilization potential of digital models, like the digital twin. It is estimated that more than 20 billion things will be connected to the internet by 2020. (Standish, 2018)

The digital twin is a model based on either a product, service or process. The digital twin also needs data for the model. In the boardmaking industry, data is typically from the physical product. The digital twin is a suitable solution for connecting the physical and digital products. They interact by sharing information. New information about the physical product helps to refine the digital model, and findings based on modelling help in optimizing the physical product. This cycle iterates both products and develops them further. The characteristics of a good digital twin are the scalability, consistency, compatibility, malleability and precision of the results. (Zheng et al., 2019)

The digital twin has many different utilization possibilities and, as a relatively new invention, new possibilities are awaitting to be discovered. The present applications are focused on the industrial field, and there is a minimal amount of consumer products. The digital twin can be used for tracking, optimizing and predicting the operation of the physical product. The digital model enables cheaper and possibly more precise testing compared to when the same operations are performed on the physical product. (Zheng et al., 2019) The digital twin developed as part of this master's thesis can perform these typical functions. It can be used to monitor the condition of the heat recovery system. A modular design allows the tracking of detected defects to a single component. Based on this process, selected key performance indicators are visualized in a user-interface.

6 HEAT RECOVERY SIMULATIONS

The behavior of the heat recovery system simulation is evaluated in this chapter. Simulations are run using the model created in this thesis. The accuracy of the model results is verified by comparing them against Valmet's heat recovery unit dimensioning tool and heat recovery model developed and presented by Leena Kilponen in her licentiate thesis. In addition, the influence of different parameters on simulation results is examined. The objective of this examination is to better understand the behavior of the model and compare the findings against known information about the heat recovery process. The results are presented as a relation to some other value, because the exact numerical values are confidential.

6.1 Verification of the simulation results

It is important to verify the model results before introducing the new model into general use. The results' accuracy must be confirmed as sufficient before the model is implemented. The results' verification provides data about their reliability, which must be accounted for in the analysis of the simulation results.

6.1.1 Comparison with Valmet's dimensioning tool

Currently, Valmet is using an internal dimensioning tool to design the heat recovery systems. The tool was developed in the 1990s and has been modified occasionally as inaccuracies have been identified. The tool was coded with FORTRAN, which is an old programming language. It was originally developed in the 1950s. (Backus, 1978) Its integration with new information systems would be problematic, and it is incompatible with available process data. A new model is therefore needed, but the old tool can be utilized in the verification of the new model. The old tool cannot be considered perfectly accurate, but its results are assumed to be in the correct range.

The comparison is made by simulating identical heat recovery towers in both the Simulink model and Valmet's dimensioning tool. The tower consists of one CHR unit which is connected in a series with two AHR units. The AHR units consist of parallel units but are modelled as a single unit. A diagram of the system is presented in figure 6.1.

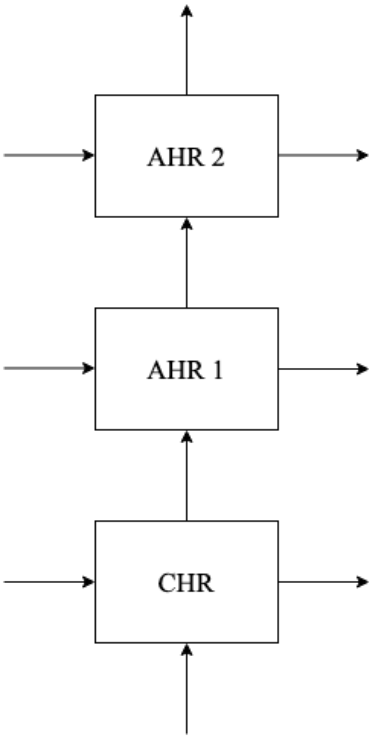

Figure 6.1. Diagram of the simulated heat recovery tower.

A comparison is made of two static cases with different input parameters but the same heat recovery unit types and connections. Input data for both cases is presented in appendix II. In addition to normal cases, both cases are also simulated with low and high exhaust air humidities. Varying humidities are designed to research the model's condensation calculation accuracy. Simulation comparison results are shown in tables 6.1-6.6. The results are presented as percentage differences between the Simulink model and the dimensioning tool. A positive value means the model's results are greater than the dimensioning tool's and negative values mean that dimensioning tool's results are greater than the model's.

Table 6.1. Comparison results for case 1.

Heat exchanger unit	Parameter	Heat emitting	Heat absorbing	Overall
CHR	Absolute humidity [g H_2O/kg d.a.]	0,38 %	0 %	
	Temperature [°C]	-0,15 %	0,60 %	
	Recovered power [kW]			3,42 %
AHR 1	Absolute humidity [g H_2O/kg d.a.]	0,24 %	NA	
	Temperature [°C]	0,17 %	-0,23 %	
	Recovered power [kW]			-0,37 %
AHR 2	Absolute humidity [g H_2O/kg d.a.]	0,29 %	NA	
	Temperature [°C]	0,20 %	-0,27 %	
	Recovered power [kW]			-0,43 %

As shown in table 6.1, the values are coherent in both the Simulink model and the dimensioning tool. The difference between every compared simulated variable is under 1 % except for the recovered power in the CHR, which is 3,42 %.

Table 6.2. Comparison results for case 1 with low exhaust air humidity.

Heat exchanger unit	Parameter	Heat emitting	Heat absorbing	Overall
CHR	Absolute humidity [g H_2O/kg d.a.]	0 %	0 %	
	Temperature [°C]	-0,34 %	2,42 %	
	Recovered power [kW]			7,21 %
AHR 1	Absolute humidity [g H_2O/kg d.a.]	1,31 %	NA	
	Temperature [°C]	0,50 %	-0,78 %	
	Recovered power [kW]			-1,51 %
AHR 2	Absolute humidity [g H_2O/kg d.a.]	-0,15 %	NA	
	Temperature [°C]	0,58 %	-0,55 %	
	Recovered power [kW]			-1,21 %

In case 1 with low humidity, the values are typically coherent between the Simulink model and the dimensioning tool, but some values differ. The CHR results differ, which can be seen especially in a CHR recovered power in table 6.2 The difference is more than 7 %. The recovered powers of both AHR units are more than 1 % less in the Simulink model than in the dimensioning tool. This is explained by the modelled CHR unit's colder exhaust air.

Table 6.3. Comparison results for case 1 with high exhaust air humidity.

Heat exchanger unit	Parameter	Heat emitting	Heat absorbing	Overall
CHR	Absolute humidity [g H_2O/kg d.a.]	-0,13 %	0 %	
	Temperature [°C]	0,07 %	1,26 %	
	Recovered power [kW]			4,43%
AHR 1	Absolute humidity [g H_2O/kg d.a.]	0,11 %	NA	
	Temperature [°C]	0,15 %	-0,13 %	
	Recovered power [kW]			-0,30 %
AHR 2	Absolute humidity [g H_2O/kg d.a.]	0,51 %	NA	
	Temperature [°C]	0,18 %	-0,14 %	
	Recovered power [kW]			-0,27 %

As shown in table 6.3, the values of the Simulink model and the dimensioning tool are relatively coherent. The differences between the compared simulated variables are mainly under 1 %, except for the supply air temperature and the recovered power in the CHR. The CHR's recovered power is the biggest difference, at 4,43 %.

Table 6.4. Comparison results for case 2.

Heat exchanger unit	Parameter	Heat emitting	Heat absorbing	Overall
CHR	Absolute humidity [g H_2O/kg d.a.]	0,17 %	0 %	
	Temperature [°C]	0,33 %	-3,34 %	
	Recovered power [kW]			-3,30 %
AHR 1	Absolute humidity [g H_2O/kg d.a.]	0,89 %	NA	
	Temperature [°C]	0,75 %	-0,60 %	
	Recovered power [kW]			-0,94 %
AHR 2	Absolute humidity [g H_2O/kg d.a.]	1,71 %	NA	
	Temperature [°C]	0,64 %	0,02 %	
	Recovered power [kW]			-0,07 %

In case 2, the values are relatively coherent for the Simulink model and the dimensioning tool. As shown in table 6.4, the differences between the compared simulated variables are mainly under 1 %. The heat exchange with the supply air is more efficient in the dimensioning tool than in the Simulink model. Supply air temperature is 3,34 % less in the model and the CHR's recovered power's difference is similar, at 3,30 %.

Table 6.5. Comparison results for case 2 with low exhaust air humidity.

Heat exchanger unit	Parameter	Heat emitting	Heat absorbing	Overall
CHR	Absolute humidity [g H_2O/kg d.a.]	0 %	0 %	
	Temperature [°C]	0,37 %	0,81 %	
	Recovered power [kW]			3,63 %
AHR 1	Absolute humidity [g H_2O/kg d.a.]	-0,53 %	NA	
	Temperature [°C]	1,10 %	-0,35 %	
	Recovered power [kW]			-1,25 %
AHR 2	Absolute humidity [g H_2O/kg d.a.]	2,57 %	NA	
	Temperature [°C]	0,94 %	0,06 %	
	Recovered power [kW]			0,54 %

As shown in table 6.5, some values are coherent in the Simulink model and the dimensioning tool, but there are also differing values. The CHR results differ, which can be seen especially in the recovered power, where the difference is 3,63 %. The recovered power of the AHR 1 is more than 1 % less in the Simulink model than in the dimensioning tool.

Table 6.6. Comparison results for case 2 with high exhaust air humidity.

Heat exchanger unit	Parameter	Heat emitting	Heat absorbing	Overall
CHR	Absolute humidity [g H_2O/kg d.a.]	0,27 %	0 %	
	Temperature [°C]	0,28 %	-3,45 %	
	Recovered power [kW]			-3,29 %
AHR 1	Absolute humidity [g H_2O/kg d.a.]	1,13 %	NA	
	Temperature [°C]	0,27 %	-0,56 %	
	Recovered power [kW]			-0,87 %
AHR 2	Absolute humidity [g H_2O/kg d.a.]	1,17 %	NA	
	Temperature [°C]	0,47 %	-0,20 %	
	Recovered power [kW]			-0,32 %

In case 2 with high humidity, the values vary more in the two simulation methods comparing with the other cases. The biggest difference is in the CHR, where the supply air temperature and recovered power results vary by more than 3 %. The big difference comparing with the other cases is the differences in humidity, where the differences are more than 1 % in both AHR units.

In general, the created model is coherent with Valmet's dimensioning tool when accounting the whole system. The CHR results differ more than the AHR results. The difference appears to be typically around 3 %, but differences are proved to increase by up to at least 7 %. The AHR model is very coherent with the dimensioning tool, where the results are typically at or below 1 %, although the difference accumulated in the CHR continues into the AHR.

6.1.2 **Comparison with model developed by L. Kilponen**

In her 2002 licentiate thesis, Leena Kilponen researched the modelling of the hood's heat recovery system. The model was originally created to simulate the Metso's paper machines at Kaipola. The licentiate thesis published the input data and the simulation

results. According to a study by Kilponen (2002), the results based on comparisons with manufacturer values were quite accurate.

The comparison with the Kilponen model is made by simulating the same kind of heat recovery stacks and using the same input data as determined in a study by Kilponen (2002). The input data is available in Kilponen (2002) and it is presented in appendix III. A comparison is made between three different paper machines as they were presented in the licentiate thesis. The simulation comparison results are shown in tables 6.7-6.9. Complete input data is given for the CHR and first AHR units, which means the differences formed in the first AHR unit continue to the second AHR unit. The results are presented as a percentage difference between the model developed in this thesis and the model developed by Kilponen (2002). A positive value means that the model's results are greater than Kilponen model's results. A negative value means that the results from Kilponen the model are greater than results from model created in this thesis.

Table 6.7. Comparison results for example paper machine 1 with the Kilponen model.

Heat exchanger unit	Parameter	Difference
CHR	Supply air temperature at outlet [°C]	-14,7 %
	Recovered power [kW]	-24,4 %
AHR 1	Process water temperature at outlet [°C]	-4,7 %
	Recovered power [kW]	-6,2 %
AHR 2	Circulation water temperature at outlet [°C]	-8,9 %
	Recovered power [kW]	-19,0 %
	Exhaust air temperature at outlet [°C]	3,8 %
	Exhaust air humidity at outlet [g H_2O/kg d.a.]	22,0 %

The example stack of paper machine number 1 consists of a CHR unit, an AHR unit for process water and an AHR unit for circulation water. The units are connected in a series in the presented order. In the CHR, both comparison values are significantly negative.

Both AHR units' differences are better than the CHR's. The first AHR unit for process water is quite coherent with the values obtained from Kilponen model. Overall, the percentage differences are bigger in recovered powers than in the corresponding heat absorbing flows' temperatures. The exhaust air temperature is higher based on the model developed in this thesis, which means that less heat is transferred into the absorbing flow. This can be seen in the negative differences in the lower absorbing flow temperatures and recovered powers in every unit.

Table 6.8. Comparison results for example paper machine 2 with the Kilponen model.

Heat exchanger unit	Parameter	Difference
CHR	Supply air temperature at outlet [°C]	-14,8 %
	Recovered power [kW]	-23,5 %
AHR 1	Circulation water temperature at outlet [°C]	0 %
	Recovered power [kW]	2,9 %
AHR 2	Process water temperature at outlet [°C]	0,1 %
	Recovered power [kW]	4,7 %
	Exhaust air temperature at outlet [°C]	-7,5 %
	Exhaust air humidity at outlet [g H_2O/kg d.a.]	-5,3 %

The example stack of the paper machine number 2 consists of a CHR unit, an AHR unit for circulation water and an AHR unit for process water. The units are connected in a series in the presented order. The biggest differences are in the CHR unit, as the modelled supply air temperature and recovered power are significantly less than the results from the Kilponen model. Contrary to the CHR results, both AHR units' results are very coherent with the Kilponen model. The exhaust air values after the stack are slightly smaller than the reference data.

Table 6.9. Comparison results for example paper machine 3 with the Kilponen model.

Heat exchanger unit	Parameter	Difference
CHR	Supply air temperature at outlet [°C]	-16,5 %
	Recovered power [kW]	-29,5 %
AHR 1	Circulation water temperature at outlet [°C]	-0,2 %
	Recovered power [kW]	-2,7 %
AHR 2	Process water temperature at outlet [°C]	0,6 %
	Recovered power [kW]	1,4 %
	Exhaust air temperature at outlet [°C]	-4,3 %
	Exhaust air humidity at outlet [g H_2O/kg d.a.]	-2,1 %

The example stack of paper machine number 3 consists of a CHR unit, an AHR unit for circulation water and an AHR unit for process water. The units are connected in a series in the presented order. Like the other comparisons, the CHR results are not coherent with the Kilponen model. The model's supply air temperature is 16,5 % less than Kilponen model's result, and the difference in recovered power is almost twice as much. The AHR results are coherent as are the exhaust air results.

Overall, CHR modelling differs more from the Kilponen model than AHR modelling when all three cases are compared. The supply air outlet temperature is lower by approximately 15 %, and the recovered power in the CHR is lower by approximately 25 %. The AHR is much more coherent, as its results typically vary less than 5 %. Th exhaust air temperature and humidity are typically quite similar with the Kilponen, model as the difference is below 10 %. The exception to this is the humidity in example paper machine 1, where the difference is more than 22 %.

6.2 Parameters influence to the model behavior

The parameters' influence on the modelling is researched by decreasing and increasing the relevant input parameter values and comparing the results to the results obtained by

the unchanged input values. This information is useful in considering possible calculation uncertainty from measuring inaccuracy. The ability to separate disturbances in a real process from measuring inaccuracy affects the data analyzation methods and findings.

A parameter influence review is done separately for CHR and AHR units that are not connected. The simulated heat recovery units are modelled based on the typical parameters for a board machine hood's heat recovery. The results for the CHR are presented in a table 6.10 and the results for the AHR are presented in a table 6.11. The results are presented as a percentage difference between the new and initial values. The single input parameter value is decreased or increased by 5 %, and its effects on all output parameters are considered. The parameters' influence on the model is reviewed for the flow rate of the emitting and absorbing flows, the temperature of the emitting and absorbing flows, the humidity of the emitting and absorbing flow. The top horizontal parameter values are changed, and the effects are seen in its column.

Table 6.10. Parameters influence on the modelling results in the CHR.

-5 %	$\dot{m}_{\text{in,emit}}$	$T_{\text{in,emit}}$	$x_{\text{in,emit}}$	$\dot{m}_{\text{in,abso}}$	$T_{\text{in,abso}}$	$x_{\text{in,abso}}$
$\dot{m}_{\text{out,emit}}$	-5 %	0 %	0 %	0 %	0 %	0 %
$T_{\text{out,emit}}$	-0,3 %	-3,6 %	-0,5 %	0,3 %	-0,2 %	0 %
$x_{\text{out,emit}}$	-0,1 %	-0,1 %	-4,9 %	0,1 %	0 %	0,1 %
$\dot{m}_{\text{out,abso}}$	0 %	0 %	0 %	-5 %	0 %	0 %
$T_{\text{out,abso}}$	-0,8 %	-4,8 %	-0,6 %	0,7 %	-0,8 %	0,1 %
$x_{\text{out,abso}}$	0 %	0 %	0 %	0 %	0 %	-5 %
P_{recov}	-1,4 %	-8,8 %	-1,1 %	-3,7	2,7 %	-0,2 %
+5 %	$\dot{m}_{\text{in,emit}}$	$T_{\text{in,emit}}$	$x_{\text{in,emit}}$	$\dot{m}_{\text{in,abso}}$	$T_{\text{in,abso}}$	$x_{\text{in,abso}}$
$\dot{m}_{\text{out,emit}}$	+5 %	0 %	0 %	0 %	0 %	0 %
$T_{\text{out,emit}}$	0,3 %	3,8 %	0,5 %	-0,3 %	0,2 %	0 %
$x_{\text{out,emit}}$	0,2 %	0,1 %	4,9 %	-0,1 %	0,1 %	0 %
$\dot{m}_{\text{out,abso}}$	0 %	0 %	0 %	+5 %	0 %	0 %
$T_{\text{out,abso}}$	0,7 %	4,6 %	0,6 %	-0,7 %	0,8 %	-0,1 %
$x_{\text{out,abso}}$	0 %	0 %	0 %	0 %	0 %	+5 %
P_{recov}	1,3 %	8,3 %	1,0 %	3,6 %	-2,7 %	0,2 %

Based on the CHR results presented in table 6.10, the recovered power is most influenced by the changes in input parameters. The mean difference for recovered power is 2.92 % when all parameters' individual influences are considered. Another significant correlation is between the temperature of the emitting flow at the inlet and the temperature of the absorbing flow at the outlet, which change by -4,8 % and 4,6 %. The significant correlation is typically with the parameter itself. For example, the emitting flow temperature at the inlet greatly affects the emitting flow temperature at the outlet. The emitting flow humidity at the inlet generates the biggest average difference in outputs.

The mean difference is 2,44 %, and the biggest influence can be seen in the recovered power, which differs by -8,8 % and 8,3 %.

Table 6.11. Parameters influence on the modelling results in the AHR.

-5 %	$\dot{m}_{\text{in,emit}}$	$T_{\text{in,emit}}$	$x_{\text{in,emit}}$	$\dot{m}_{\text{in,abso}}$	$T_{\text{in,abso}}$	$x_{\text{in,abso}}$
$\dot{m}_{\text{out,emit}}$	-5 %	0 %	0 %	0 %	0 %	0 %
$T_{\text{out,emit}}$	-0,6 %	-2,3 %	-1,2 %	0,5 %	-0,3 %	-0,1 %
$x_{\text{out,emit}}$	-1,4 %	-0,8 %	-5,3 %	1,3 %	-0,7	-0,2 %
$\dot{m}_{\text{out,abso}}$	0 %	0 %	0 %	-5 %	0 %	0 %
$T_{\text{out,abso}}$	-0,2 %	-0,4 %	-1,5 %	0,2 %	-0,1 %	0,1 %
$x_{\text{out,abso}}$	0 %	0 %	0 %	0 %	0 %	-5 %
P_{recov}	-0,3 %	-0,7 %	-2,3 %	-4,7 %	2,4 %	0,5 %
+5 %	$\dot{m}_{\text{in,emit}}$	$T_{\text{in,emit}}$	$x_{\text{in,emit}}$	$\dot{m}_{\text{in,abso}}$	$T_{\text{in,abso}}$	$x_{\text{in,abso}}$
$\dot{m}_{\text{out,emit}}$	5 %	0 %	0 %	0 %	0 %	0 %
$T_{\text{out,emit}}$	0,6 %	2,3 %	1,1 %	-0,5 %	0,3 %	0,1 %
$x_{\text{out,emit}}$	1,2 %	0,7 %	5,3 %	-1,3 %	0,7 %	0,1 %
$\dot{m}_{\text{out,abso}}$	0 %	0 %	0 %	5 %	0 %	0 %
$T_{\text{out,abso}}$	0,2 %	0,5 %	1,5 %	-0,2 %	0,1 %	-0,1 %
$x_{\text{out,abso}}$	0 %	0 %	0 %	0 %	0 %	5 %
P_{recov}	0,3 %	0,7 %	2,2 %	4,6 %	-2,4 %	-0,5 %

The results from the AHR parameter influence review are mostly similar to those from the CHR. The AHR results are presented in table 6.11, where the recovered power is most influenced by changes in input parameters. In addition, the humidity of the emitting flow at the outlet differs more than the average value. Another significant correlation is between the temperature of the emitting flow at the inlet and the temperature of the absorbing flow at the outlet, where the changes are -5,3 and 5,3 %. Obviously, the significant correlation is typically with the parameter itself. For example, the emitting

flow temperature at the inlet greatly affects the emitting flow temperature at the outlet. The emitting flow temperature at the inlet generates the biggest average difference in outputs. The mean difference is 1,44 %, and the biggest influence can be seen in the emitting flow humidity at the outlet, which differs by -5,3 % and 5,3 %. The biggest influence on the recovered power is from absorbing flow rate, which results in a change of a little less 5 % in recovered power.

7 CUSTOMER APPLICATION

The customer demand for industrial internet applications is increasing, and data utilization overall is being embraced in the current technology field. One of Valmet's solutions for using data to improve the board machine is to use a digital twin in machine optimization. A digital twin will be created for the all machine sections of board making process. This thesis focuses on the drying section hood area. The model will be used as a core for the heat recovery system digital twin. The customer MVP and the potential uses of this tool are presented in this chapter.

In the first version of the development, the application will be an MVP. The application will consist of two analyzing methods: a model for heat recovery and monitoring of key performance indicators (KPIs). The additional features and available options may be added in future, depending on customer needs. Future development plans will be based on user experience of the MVP. The model can be used to simulate the different conditions or compare the modelled results to the measurements. Simulation possibility is important, because it enables the testing of the machine without affecting the actual process. Modelling is required when trying to optimize heat recovery in context with the entire boardmaking process. The goal will thus not be to maximize the recovered energy but to minimize energy consumption in relation to production quantity and quality. In addition, modelled values can be compared to measured ones, and recognize abnormalities in the actual process. For example, the condition of the equipment can be monitored by comparing its performance against model. The difference in model-measurement provides data for maintenance needs. Another way to monitor the condition of the process is to track certain KPIs. KPIs can be compared against limits that are based on their history data or dimensioning. These limits form the criteria for where the KPI values must be for enable efficient board production with efficient heat recovery. The location of the KPI in the limit scale is visualized using the traffic light color signs where green means good, yellow means that the value must be monitored and red indicates a bad status when actions are needed to improve the situation. The app also contains operating instructions. The instructions offer suggestions concerning what changes should be made to restore the good state again. Instructions are offered when the indicator is at yellow or red.

The MVP customer application is made using Amazon Web Services (AWS). AWS is a cloud computing platform service from Amazon. AWS provides technical and distributed infrastructure, which can be utilized for on-line software, as with the application developed in this thesis. (Shackelford 2015, 1-2) The visualization of the app is made using Tableau. Tableau is a business intelligence platform that is designed for visualizing data using interactive dashboards. (Hardy, 2014) Tableau is utilized in many of Valmet's industrial internet applications because of its good connectivity in the interfaces.

The application created in this thesis is part of a bigger digital twin application family, which sets certain boundary conditions for its structure and the visualization. The structure is three staged to ensure sufficient coherence with other applications. In addition, visualization is determined by pre-set graphical instructions from Valmet and Tableau restrictions. The first stage consists of all the digital twins, and the corresponding traffic light colors indicate every section's state. The condition is defined by a combination of the KPIs. The second stage is a landing page, when for example heat recovery, is selected. The landing page consists off a process diagram, which shows the states of the different sections or equipment, and links to the third stage. The application's third stage contains more detailed information. It focuses on a specific examination of the KPIs. At this stage, the exact values of the measurements are presented. The visualization methods are bar meters, which visualize condition using traffic light colors, and x-y-plots, which visualize the history trends. In addition to the visualization methods that describe the condition of the measurement, operation instructions are suggested for correcting the system's inefficient operation.

The third stage of the app is where the actual calculated and measured numerical values are presented. The four monitored values are chosen to be presented, which are the heat recovery efficiency indicator, the recovered energy, the recovered power versus the consumed steam power and the heat recovery coil cleanliness. All these are visualized using a numerical value, bar meter and trend in the x-y-axis. The heat recovery efficiency indicator is calculated as presented in chapter 5.1.3, and the limits for the traffic lights are defined based on historically achieved data in certain conditions. The recovered energy can be monitored based on a model or measurements. The limits are defined by nominal values, making the yellow and red limits to be a certain percentage below the nominal

value. Certain conditions must also be considered when defining these limits. For example, the outside temperature affects the heating need. The recovered power versus steam consumption is obtained by comparing their respective measurements and the limits are defined based on nominal values in the same way as in the case of recovered energy. The heat recovery coil cleanliness is monitored by observing the operation of the blower. When the blower diverges from the nominal curve, the coil cleanliness must be checked. The limits are defined based on empirical testing.

The application is sold to customers as a part of the company's other industrial internet products. The heat recovery application is mainly used by machine operators to achieve the best possible production with minimal energy consumption. When more complex analyzing tools are implemented in the application, the target user group will widen to include experts and other white-collar workers. The user group affects the appearance of the application. On the landing page, the process diagram is chosen to lower the threshold for the operator to use the app. The process diagram is thought to be the best way to approach the tool.

8 FINDINGS AND CONCLUSIONS

The conclusions of this thesis are presented in this chapter. In the case of model validation, this entails an analysis of the modelling results. In the case of the customer application, it refers to the customer utilization possibilities. The heat recovery system in board machines has received a little attention from the new analyzation methods. Data is underutilized in heat recovery compared to other processes in the boardmaking process. Because of the minimal attention and the process' complexity, there is no universally accepted model for a heat recovery system. Some research is published on this topic, but an unambiguous solution for modelling has not been presented. The board machine heat recovery modelling was researched in a study by Kilponen (2002) and additional research was needed according its conclusions. Her focus was on developing an accurate model, which could be used for existing heat recovery system optimization. The conclusions of this thesis are compared with Kilponen's findings. In addition, challenges are presented, and future subjects for discussion are suggested in this chapter.

8.1 Heat recovery simulation

The heat recovery system model is created from Simulink block library developed in this thesis. It is used as a dimensioning tool for designing the system and as an analyzation and optimization tool for the operating the machine. The problem before the launch for utilization can happen is the validation of the model accuracy. No board machine has sufficient measurements for model verification. Mainly, water temperature measurements before and after the recovery units are missing but also temperature measurements on heat emitting air stream are typically missing. Model is validated by comparing it against other developed models. The model was compared against Valmet's dimensioning tool and model created in a study by Kilponen (2002). The comparison was made to provide a rough estimate of the created model's accuracy.

The comparison with Valmet's dimensioning tool was implemented using two heat recovery system cases with typical input parameters. In addition, both cases were calculated using low and high exhaust air humidity to obtain a better understanding of model behavior, and especially of condensation. Condensation modelling was considered a problem because of its big impact on heat recovery and possibility for condensates

draining on the heat exchange surfaces. The results of the comparison are presented in tables 6.1-6.6. Two main conclusions are drawn from this: the models differ more in CHR units than AHR units and the difference between models was not a constant. A bigger variance in CHR modelling was forecasted, because the heat transfer method on the air side varies between convection and condensation, which increases the demand for model precision. Another finding from this comparison was that the difference varies. The values from this model were sometimes smaller and sometimes bigger than the values obtained from the dimensioning tool. The reason for this is difficult to identify, because it has not been possible to test either methods against the measured data.

Another comparison for the model was against the model developed in a study by Kilponen (2002). A simulation was made using three paper machine examples. Input parameters were presented in the Kilponen licentiate thesis. The comparison results are presented in tables 6.7-6.9. The results were in some parts similar to the comparison with dimensioning tool. The main observation was a difference in CHR modelling, as was also observed in the dimensioning tool comparison. In this comparison, the differences were bigger than in the case of the dimensioning tool. CHR values differ by between 14 % and 30 %, and the Kilponen model values were always higher than those obtained from created model. The singular major differences were in the recovered power from the circulation water AHR unit and the exhaust air humidity after the same unit. Typically, AHR modelling seems to be coherent with both the dimensioning tool and Kilponen's model. The simulation results from three different calculations were similar, meaning the AHR model's reliability can be considered significantly better than the CHR model's.

The results indicate that the modelling is generally in line with other models. However, the model cannot be trusted as an absolutely accurate, and possible error must be considered when utilizing it. Based on the comparisons, the AHR model is more accurate than the CHR model. Typically, the AHR results differ by 5 % or less compared with the other models. The CHR usually differs by 5-10 %, but occasionally up to 30 %. Additional testing is needed for the findings to have more significance. The CHR model's challenges are expected, as condensation is more difficult to model accurately. Condensate draining onto the heat exchange surface causes inaccuracy to increase. In modern board machines, the CHR unit is typically connected first, followed by the AHR

units in a series. This causes modelling inaccuracies formed in the CHR unit to continuing to the AHR units, which reduces the overall model's the reliability. Fortunately, the recovered energy in the AHR units is superior to recovered energy in the CHR unit, which decreases the inaccuracy of the overall system modelling when the system is considered as a single unit.

During additional tests when building and validating the model, model was noticed to give more recovered energy than the measurements indicate. One reason for this difference may be inconsistent conditions on the heating surface. Model is simplified to the one-dimensional case, but the reality is a multi-dimensional. For example, distorting flow profiles at the curves increase the uncertainty of the modelling as the one-dimensional model does not consider that. Must be noted, that multiple necessary measurements were missing, decreasing the significance of this notion.

Modelling behavior was researched from the perspective of input parameters. The research was based on typical CHR and AHR units, which were simulated using typical input parameter values. The results were compared against the results obtained from a simulation in which one of the parameter's value was increased and decreased by 5 %. The most influential parameters in the CHR unit were the emitting flow inlet temperature, the absorbing flow inlet flow rate and the absorbing flow inlet temperature. The most influential parameters for the AHR unit were the absorbing flow inlet flow rate, the absorbing flow inlet temperature and the emitting flow inlet humidity. The criterion for how influential they are, is the effect on the recovered power, because recovering of power is the main purpose of the heat recovery system. The conclusions would change only a little if the influence on all the results were considered. When the entire system is considered, the influential parameters for the AHR unit are more significant than the CHR's, because most of the recovered power is recovered in the AHR units. Most of the recovered power is transferred with condensation, meaning the parameters that increase condensation, are important. Exhaust air humidity is important, because the humidity increases the dew point, which increases the potential for condensation. Another important parameter for condensation is a low inlet temperature for the absorbing flow, which lengthens the duration of the condensation.

The model will be used in analyzing the heat recovery system performance and in system dimensioning. Multiple utilization purposes demand certain adaptations to the model. The big difference between the two purposes is calculation time demand. The on-line AWS application needs smooth operating from the model, the exact demand for calculation time is dependent on used data sampling interval. The heat recovery system is a comparatively stabile process, the data sample interval does not need to be particularly short. A one-minute interval is sufficient for the heat recovery system, so the calculation must be completed in less than one minute. The example cases used in this thesis were consisted of one CHR unit and two AHR units in a series. They were modelled in approximately 20-25 seconds, with the CHR modelling grid being 30x30. Computational power must be accounted for, because lighter models are preferred in cloud services. Quick computation is required when the model is used as a dimensioning tool, which allows the designer to quickly run through multiple scenarios. Changing the grid size affects the computation time. Example of this is presented in the appendix I. Making the grid smaller decreases the calculation time. Making the grid size denser increases computation time, but it enables more accurate results that is necessary when doing the final design.

Development of a graphical user interface for the hood's heat recovery system would be helpful in the practical use of the model according to Kilponen (2002). This need is fulfilled in this thesis, as the model was made in Simulink, where CHR and AHR blocks form a block library for heat recovery. In Simulink, blocks can be freely moved and connected in any way the user wants in a graphical user interface. This means that the heat recovery system design models are simple to build and rearrange. This is an essential attribute, because this model is intended to be used as a dimensioning tool for the heat recovery system designing process. The interface must be simple to use, which Simulink provides.

8.2 Customer application

The customer application as a sellable product is mapped out in this thesis. The application is used to monitor the heat recovery process on-line. The state of the process

is indicated by calculated values and KPIs. The designed limits determine the traffic light colors, which are used to indicating the state of the process.

The main use of the application is the optimization and condition monitoring of the board machine's heat recovery system. The focus is especially on machines that are in operation. The three main uses for the application are:

- In identifying if the system is working as designed;
- In monitoring the condition of the equipment;
- In optimizing the system so that the efficiency of the process increases.

Valmet has unique knowledge of the planned functioning of the heat recovery system because of Valmet's designing of its own machines. Therefore, the application offers direct know-how to the customer that would otherwise be unattainable. This can be interpreted from the traffic light colors as the multiple limits are based on nominal dimensioned values. In addition, the performance of the controlling circuits, for example, can be distinguished from the oscillation of the measurements. The conditions of the equipment can be observed from multiple indicators. A low heat recovery efficiency indicator value, low recovered energy or inefficiently functioning fan may all indicate that equipment needs maintenance. An example of this is when there is a yellow or red light in heating coil cleanliness indicator. This means the coil's cleanliness must be checked. The optimizing of the heat recovery system is possible with a test simulation using the heat recovery model created in this thesis or simply by monitoring chosen KPIs with the app. The monitoring of the KPIs enables quicker action to correct the cause of the problem. The app includes operation instructions for each indicator independently. A major improvement in problem solving efficiency is possible to achieve by obtaining information about the state of the system in real time with additional operation instructions telling the needed actions.

Created model's use in system designing is supporting the customer product. When certain machine's heat recovery system is designed with Simulink model, the model for the system is formed already and additional work for building the model is not needed. In addition to saving time in not having to build the model, dimensioning information can be included to the product, telling operator how the equipment is designed to be operated.

The optimization of the system operation and quicker reactions to problems both benefit the boardmaking company by making the production process more efficient. These benefits can be realized as an increased production rate, which increases the quantity of the sellable product, decreased energy consumption thereby decreasing the board machine's operation costs and possibly decreasing the emissions, depending on the energy production method. The often-disregarded decrease in overall emissions is likely to be more important in the future.

8.3 Challenges and future discussion

The main challenge for this thesis was the validation of the created model. Economic challenges in boardmaking during last years have led to machines with low instrumentation and a shortage of measurements. Modelled values cannot be compared against measured values, which would provide valuable data for the validation of model accuracy.

Because of the missing measurements, validation is performed by comparing the model results against the results from other models. Modelling results can usually be trusted to give a general idea about the system operation, but more testing is needed to enhance and ensure the reliability of the model. The reliability of the current model is not good enough for it to be used as a dimensioning tool. The best way to validate the model is to compare the modelled results against measured results, but if measurements are unavailable, testing can be performed by simulating multiple reference points from multiple machines. A bigger reference group would increase the accuracy of the estimation.

Comprehensive measurements are needed for model validation and utilization as an analyzation tool. Temperature measurements before and after heat exchangers are often missing as they are relatively expensive to measure, especially in water flows. Measuring devices are not themselves expensive, but when installation, documentation and automation system change costs are added, the overall investment increases. A possible solution for the lack of measurements is to utilize measuring devices that are sending signals directly to a cloud service. This would be bypassing the automation system, making savings in documentation costs. Such an idea might also be implemented by buying the service from an external subcontractor. The subcontractor would then be

responsible for transferring the data to the cloud service. Although this is a promising idea, it has not yet to be implemented at Valmet, because the operation and business aspects require more research before utilization.

9 SUMMARY

Boardmaking starts during pulping. Additives are added to the pulp, and after the pulp is handled in certain components, it is called stock. Stock is dried and processed at the board machine, which consists of a former, press, dryer, sizer, calender, reel and winder. Water removal from the drying section occurs by evaporation, and the drying section is covered with a hood, which prevents the moist air from moving to the machine hall. Evaporated water is removed from the hood by ventilation. Warm and moist air contains a lot of heat, which is cycled through the heat recovery system. Recovered heat is utilized in heating the different air and water flows, lowering the board machine's primary energy consumption.

A modern heat recovery system consists of two types of heat recovery units: the CHR for air-to-air heat recovery and the AHR for air-to-water heat recovery. In the CHR, heat is transferred from the exhaust air to the heating surface partly by convection and partly by condensation. From the heating surface, the heat is transferred by convection to the absorbing air flow. In the AHR, heat is transferred from the exhaust air to the heating surface by convection. From the heating surface, the heat is transferred by condensation to the absorbing water flow. Both units were modelled independently using MATLAB, and they form corresponding blocks in Simulink. The models were validated by comparing them to existing heat recovery models. Valmet's heat recovery system design tool and the heat recovery model developed in a study by Kilponen (2002) were used as reference models. The CHR was found to being less accurate than the AHR, which was explained by the heat transfer in the emitting side. In the CHR, heat was transferred either by convection or condensation, depending on humidity and temperatures. The CHR results differed typically 5-10 % from the reference models, but the difference could be as much as 30 %. The AHR difference was typically below 5 %.

The input parameters' influence on model behavior, and especially on recovered power, was researched. Parameters that lead to increasing condensation were found to be the most important, as the heat transfer is more efficient by condensation than convection.

The created CHR and AHR models will be used as a digital twin for the heat recovery system. The digital twin is part of the MVP customer application, which was brainstormed

in this master's thesis. The application will be used to monitor the condition of the heat recovery system, with the objective of enabling optimized use. In addition, the application will enable trouble-shooting for internal operations.

The core idea of this thesis was to create a model for a heat recovery system for Valmet that could be utilized in various ways. Three objectives were set for the thesis. They were:

1. To create a model for a heat recovery system that indicates the system's condition, and one that is possible to convert to an on-line customer application;
2. To create a preliminary design for a customer application;
3. To create a model that can be utilized in heat recovery system designing.

The objectives of this thesis were mostly achieved, but some aspects remain to be determined in future. The first objective, which was to create a model for a heat recovery system that indicates the system's condition and one that is possible to convert to an on-line customer application, was achieved. A MATLAB model was created for the CHR and AHR units. The models' computational time was sufficient for real-time use, and building of customer application will start at the beginning of August 2019. The second objective, creating a preliminary design for a customer application, was fully achieved. The application will be based on the preliminary design described in chapter 7. The third objective was to create a model that can be utilized in heat recovery system designing. The achievement status of this goal remains to be determined. The created model can be used in designing a heat recovery system, but validation uncertainty remains a problem. The accuracy of the model may or may not be sufficient for the designing.

The verification of model accuracy proved only partly possible in this thesis. The direction of the results was good, but more precise information on model accuracy will be needed in future. Additional validation may be achieved by adding more measuring devices and comparing modelled and measured values, or by comparing modelled values with more reference data points from other models.

REFERENCES

Backus, J. 1978. Paper: The history of FORTRAN I, II and III. ACM SIGPLAN Notices, 13(8), pp. 165-180. Available at: https://doi.org/10.1145/960118.808380

Colgren, R. 2005. Basic MATLAB, Simulink, and Stateflow. American Institute of Aeronautics and Astronautics. pp. 423. ISBN 978-1-56347-838-3

Fardim, P. 2011. Chemical Pulping Part 1, Fibre Chemistry and Technology. Porvoo: Bookwell Oy. Paper Engineers' Association/Paperi ja Puu. pp. 748. ISBN 978-952-5216-41-7

Fuller, E.N., Schettler, P.D., Giddings, J.C. 1966. A new method for prediction of binary gas-phase diffusion coefficients. Industrial & Engineering Chemistry. American Chemical Society. pp. 18-27. Available at: https://doi.org/10.1021/ie50677a007

Ghoshdastidar, P.S. 2012. Heat Transfer. 2nd Edition. New Delhi: Oxfords University Press. pp. 613. ISBN 978-1-62870-851-6

Gulsoy, S.K., Kustas, S., Erenturk, S. 2013. The effect of old corrugated container (OCC) pulp addition on the properties of paper made with virgin softwood kraft pulps. BioResources, 8(4), pp. 5842-5849. Available at: https://doi.org/10.15376/biores.8.4.5842-5849

Hardy, Q. 2014. Tableau software helping data become more visual. The New York Times. [web article] [Referred 15.7.2019] Available at: https://bits.blogs.nytimes.com/2014/06/13/tableau-software-helps-data-become-more-visual/

Incropera, F. et al. 2016. Principles of Heat and Mass Transfer. Seventh Edition. New Delhi: Wiley. pp. 1048. ISBN 978-81-265-4273-4

Karlsson, M. 2009. Papermaking Part 2, Drying. Jyväskylä: Gummerus Oy. Finnish Paper Engineers' Association/TAPPI. pp. 634. ISBN 978-952-5216-37-0

Kilponen, L. 2002. Improvement of Heat Recovery in Existing Paper Machines. Licentiate's thesis. Helsinki University of Technology.

KnowPap. Paperitekniikan ja tehtaan automaation oppimisjärjestelmä: (LUT). Prowledge Oy, VTT Industrial Systems.

Lönnberg, B. 2009. Mechanical Pulping. Jyväskylä: Gummerus Oy. Paper Engineers' Association/Paperi ja Puu. pp. 549. ISBN 978-952-5216-35-6

Paulapuro, H. 2007. Papermaking Part 1, Stock Preparation and Wet End. Jyväskylä: Gummerus Oy. Finnish Paper Engineers' Association/Paperi ja Puu. pp. 516. ISBN 978-952-5216-25-7

Pita, 2016. Glossary of Papermaking Terms. [online page] [Referred 13.4.2019] Available at: https://www.pita.org.uk/images/PDF/Glossary_of_Terms.pdf

Portney, K.E. 2015. Sustainability. Cambridge, Massachusetts: The MIT Press. pp. 235. ISBN 978-0-262-33141-8

Princeton University. 1996. The Pulp and Paper Making Processes. Chapter 2. [web document] [Referred 27.6.2019] Available at: https://www.industryweek.com/technology-and-iiot/congratulations-its-digital-twin

Rautiainen, P. 2009. Papermaking Part 3, Finishing. Jyväskylä: Gummerus Oy. Finnish Paper Engineers' Association/TAPPI. pp. 404. ISBN 978-952-5216-36-3

Ryti, H. 1975. Tekniikan käsikirja 2. Jyväskylä: Gummerus. pp. 777. ISBN 951-20-1075-5

Ryti, H. 1981. Tekniikan käsikirja 1. Jyväskylä: Gummerus. pp. 566. ISBN 951-20-1074-7

Shackelford, A. 2015. Beginning Amazon Web Services with Node.j.s. Berkeley, California: Apress. pp. 237. ISBN 978-1-4842-0653-9

Sivill, L., Ahtila, P., Taimisto, M. 2005. Thermodynamic simulation of dryer section heat recovery. Applied Thermal Engineering, 25(8-9), pp. 1273-1292. Available at: https://doi.org/10.1016/j.applthermaleng.2004.09.002

Standish, R. 2018. Congratulations, It's a Digital Twin!. Industry Week. [web article] [Referred 12.6.2019] Available at: https://www.industryweek.com/technology-and-iiot/congratulations-its-digital-twin

Villalobos, J.A. 1985. Paper machine hoods, pocket ventilation, heat recovery and thru-dryers. Practical aspects of pressing and drying seminar. Atlanta: Tappi Press.

Yendler, B. 1994. A Computer Program for Condensing Heat Exchanger Performance in the Presence of Noncondensable Gases. NASA. [web article] [Referred 27.6.2019] Available at: https://www.researchgate.net/publication/24302797_A_computer_program_for_condensing_heat_exchanger_performance_in_the_presence_of_noncondensable_gases

Zheng, Y., Yang, S., Huanchong, C. 2019. An application framework of digital twin and its case study. Journal of Ambient Intelligence and Humanized Computing, 10(3), pp. 1141-1153. Available at: https://doi.org/10.1007/s12652-018-0911-3

APPENDIX I: GRAPH FOR DETERMINING THE GRID SIZE

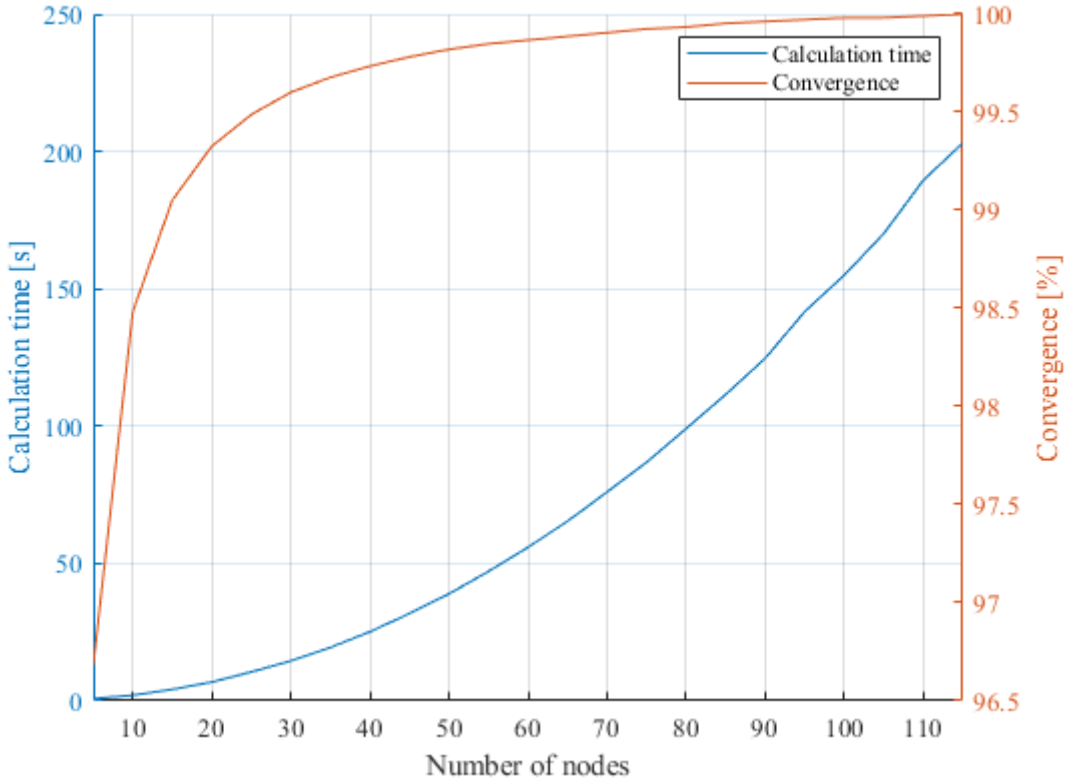

APPENDIX II: INPUT DATA FOR COMPARISON WITH VALMET'S DIMENSIONING TOOL

Input data for case 1

Heat exchanger unit	Input parameter	Value
CHR	Plate length [mm]	3950
	Plate height [mm]	1600
	Plate slit exhaust [mm]	15
	Plate slit supply [mm]	14
	Number of plates	166
	Exhaust flow rate [kg d.a./s]	50
	Absolute humidity at exhaust [g H_2O/kg d.a.]	160/50/230
	Exhaust temperature [°C]	85
	Supply flow rate [kg d.a./s]	30
	Absolute humidity at supply [g H_2O/kg d.a.]	20
	Supply temperature [°C]	28
AHR 1	Unit type	Type 2
	Parallel units	4
	Air flow rate [kg d.a./s]	input from CHR
	Absolute humidity [g H_2O/kg d.a.]	input from CHR
	Air temperature [°C]	input from CHR
	Water flow rate [kg/s]	30
	Water glycol content [%]	0
	Water temperature [°C]	20
	Unit type	Type 2
	Parallel units	4

	Air flow rate [kg d.a./s]	input from AHR 1
AHR 2	Absolute humidity [g H_2O/kg d.a.]	input from AHR 1
	Air temperature [°C]	input from AHR 1
	Water flow rate [kg/s]	30
	Water glycol content [%]	20
	Water temperature [°C]	20

Input data for case 2

Heat exchanger unit	Input parameter	Value
	Plate length [mm]	3950
	Plate height [mm]	950
	Plate slit exhaust [mm]	10
	Plate slit supply [mm]	16
	Number of plates	136
CHR	Exhaust flow rate [kg d.a./s]	30
	Absolute humidity at exhaust [g H_2O/kg d.a.]	170/50/230
	Exhaust temperature [°C]	80
	Supply flow rate [kg d.a./s]	15
	Absolute humidity at supply [g H_2O/kg d.a.]	20
	Supply temperature [°C]	22
	Unit type	Type 2
	Parallel units	2
	Air flow rate [kg d.a./s]	input from CHR
AHR 1	Absolute humidity [g H_2O/kg d.a.]	input from CHR
	Air temperature [°C]	input from CHR

	Water flow rate [kg/s]	40
	Water glycol content [%]	0
	Water temperature [°C]	22
AHR 2	Unit type	Type 2
	Parallel units	2
	Air flow rate [kg d.a./s]	input from AHR 1
	Absolute humidity [g H_2O/kg d.a.]	input from AHR 1
	Air temperature [°C]	input from AHR 1
	Water flow rate [kg/s]	25
	Water glycol content [%]	20
	Water temperature [°C]	25

APPENDIX III: INPUT DATA FOR COMPARISON WITH KILPONEN MODEL

Input data for paper machine example 1

Heat exchanger unit	Input parameter	Value
CHR	Heat ransfer area [m^2]	2152
	Plate slit exhaust [mm]	15
	Plate slit supply [mm]	11
	Exhaust flow rate [kg d.a./s]	49,8
	Absolute humidity at exhaust [g H_2O/kg d.a.]	160
	Exhaust temperature [°C]	82
	Supply flow rate [kg d.a./s]	39,9
	Absolute humidity at supply [g H_2O/kg d.a.]	20
	Supply temperature [°C]	28
AHR 1	Unit type	Type 1
	Parallel units	6
	Air flow rate [kg d.a./s]	49,8
	Absolute humidity [g H_2O/kg d.a.]	154,9
	Air temperature [°C]	67,6
	Water flow rate [kg/s]	50
	Water glycol content [%]	0
	Water temperature [°C]	15
AHR 2	Unit type	Type 2
	Parallel units	6x2
	Air flow rate [kg d.a./s]	input from AHR 1
	Absolute humidity [g H_2O/kg d.a.]	input from AHR 1

	Air temperature [°C]	input from AHR 1
	Water flow rate [kg/s]	105
	Water glycol content [%]	20
	Water temperature [°C]	23

Input data for paper machine example 2

Heat exchanger unit	Input parameter	Value
CHR	Heat ransfer area [m^2]	2288
	Plate slit exhaust [mm]	14
	Plate slit supply [mm]	14
	Exhaust flow rate [kg d.a./s]	70,6
	Absolute humidity at exhaust [g H_2O/kg d.a.]	160
	Exhaust temperature [°C]	82
	Supply flow rate [kg d.a./s]	35
	Absolute humidity at supply [g H_2O/kg d.a.]	20
	Supply temperature [°C]	28
AHR 1	Unit type	Type 2
	Parallel units	7
	Air flow rate [kg d.a./s]	70,6
	Absolute humidity [g H_2O/kg d.a.]	158,6
	Air temperature [°C]	68,9
	Water flow rate [kg/s]	187
	Water glycol content [%]	20
	Water temperature [°C]	29,9
	Unit type	Type 2

	Parallel units	7
	Air flow rate [kg d.a./s]	input from AHR 1
AHR 2	Absolute humidity [g H_2O/kg d.a.]	input from AHR 1
	Air temperature [°C]	input from AHR 1
	Water flow rate [kg/s]	50
	Water glycol content [%]	0
	Water temperature [°C]	5

Input data for paper machine example 3

Heat exchanger unit	Input parameter	Value
	Heat ransfer area [m^2]	2416
	Plate slit exhaust [mm]	13
	Plate slit supply [mm]	16
CHR	Exhaust flow rate [kg d.a./s]	69,3
	Absolute humidity at exhaust [g H_2O/kg d.a.]	160
	Exhaust temperature [°C]	82
	Supply flow rate [kg d.a./s]	45
	Absolute humidity at supply [g H_2O/kg d.a.]	20
	Supply temperature [°C]	30
	Unit type	Type 2
	Parallel units	6
	Air flow rate [kg d.a./s]	69,3
AHR 1	Absolute humidity [g H_2O/kg d.a.]	158,5
	Air temperature [°C]	67,1
	Water flow rate [kg/s]	189

	Water glycol content [%]	20
	Water temperature [°C]	30
AHR 2	Unit type	Type 2
	Parallel units	6
	Air flow rate [kg d.a./s]	input from AHR 1
	Absolute humidity [g H_2O/kg d.a.]	input from AHR 1
	Air temperature [°C]	input from AHR 1
	Water flow rate [kg/s]	66
	Water glycol content [%]	0
	Water temperature [°C]	5